Available online at www.sciencedirect.com
SCIENCE DIRECT®
Journal of Sound and Vibration 282 (2005) 575–616
JOURNAL OF SOUND AND VIBRATION
www.elsevier.com/locate/jsvi

Review

An overview of modeling and experiments of vortex-induced vibration of circular cylinders

R.D. Gabbai, H. Benaroya*

Department of Mechanical and Aerospace Engineering, Rutgers University, Piscataway, NJ 08854-8058, USA

Received 9 October 2003; accepted 13 April 2004
Available online 11 November 2004

Abstract

This paper reviews the literature on the mathematical models used to investigate vortex-induced vibration (VIV) of circular cylinders. Wake-oscillator models, single-degree-of-freedom, force–decomposition models, and other approaches are discussed in detail. Brief overviews are also given of numerical methods used in solving the fully coupled fluid–structure interaction problem and of key experimental studies highlighting the nature of VIV.

Contents

*Corresponding author. Tel.: +1-732-445-4408.
E-mail address: benaroya@rci.rutgers.edu (H. Benaroya).

0022-460X/$ - see front matter © 2004 Elsevier Ltd. All rights reserved.
doi:10.1016/j.jsv.2004.04.017

1. Introduction

Vortex-induced vibration (VIV) occurs when shedding vortices (a von Kármán vortex street) exert oscillatory forces on a cylinder in the direction perpendicular to both the flow and the structure. The structure starts to oscillate due to these forces if it is not fixed. For fixed cylinders, the vortex-shedding frequency is related to the non-dimensional Strouhal number. The Strouhal number is defined as $S = f_v D/U$, where f_v is the predominant frequency of vortex shedding. U is the steady velocity of the flow, and D is the diameter of the cylinder. The Strouhal number is found to be nearly constant with a value of 0.2 for a large range of Reynolds numbers. This range is often called the subcritical range and spans the Reynolds number range of 300–2×10^5 [1].

For flow past cylinders that are free to vibrate, the phenomenon of synchronization or lock-in is observed. For low flow speeds, the vortex-shedding frequency f_v will be the same as that of a fixed cylinder. This frequency is fixed by the Strouhal number. As the flow speed is increased, the shedding frequency approaches the vibration frequency of the cylinder f_0. In this regime of flow speeds, the vortex-shedding frequency no longer follows the Strouhal relationship. Rather, the shedding frequency becomes "locked-in" to the oscillation frequency of the cylinder (i.e., $f_0 \approx f_v$). If the vortex-shedding frequency is close to the natural frequency of the cylinder f_n, as is often the case, large body motions are observed within the lock-in regime (the structure undergoes near-resonance vibration).

It is also well known that a hysteresis behavior may exist in the amplitude variation and frequency capture depending on the approach to the resonance range—whether from a low velocity or from a high velocity [2]. As will be discussed later, the two branches of this hysteresis loop are associated with different vortex-shedding modes and transition between these branches is associated with a phase jump of $\sim 180^\circ$ [3]. Shown in Fig. 1 is a typical response in the lock-in region of a freely vibrating circular cylinder with light damping. The hysteresis effect is clearly seen, with higher amplitudes achieved when the reduced velocity is increased over a certain range. Also seen is the lock-in phenomenon, with the vortex-shedding and body oscillation frequencies collapsing into a single frequency close to the natural frequency of the cylinder. The straight line $S = 0.198$ is the line of constant Strouhal number.

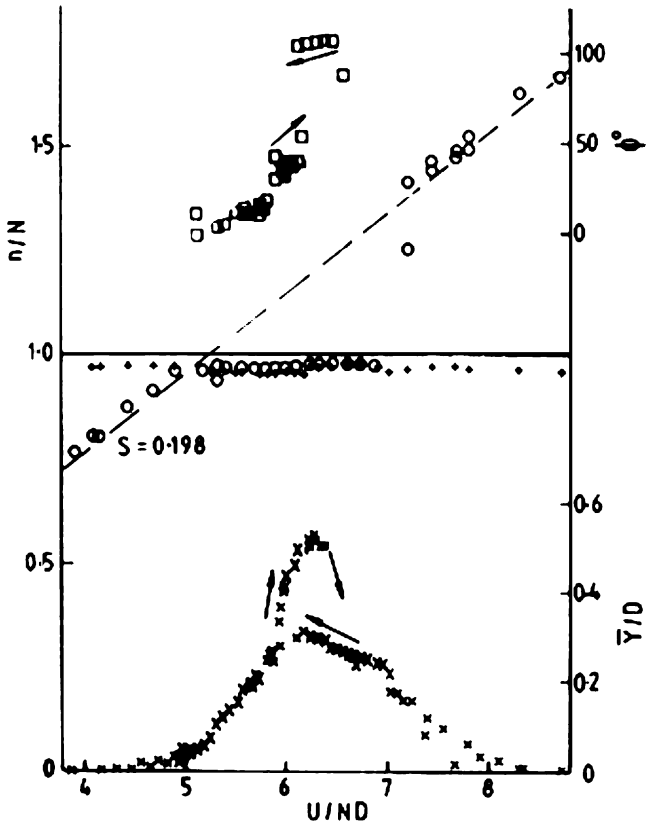

Fig. 1. Oscillation characteristics for a freely vibrating circular cylinder with light damping. N is the body oscillation frequency, n is the vortex shedding frequency, $\bar{Y}/D$ is the normalized maximum amplitude of oscillation measured at a particular value of the reduced velocity, and ϕ° is the phase angle between the fluid force and the cylinder displacement. ◯, vortex-shedding frequency; +, cylinder frequency; □, phase angle; ×, oscillation amplitude [5].

The amplitude of the structural response during lock-in and the band of fluid velocities over which the lock-in phenomenon exists is strongly dependent on a reduced damping parameter expressing the ratio of the damping force to the excitation force. The Scruton number, $Sc = 4\pi m\zeta/\rho D^2$, is but one of many representations for this reduced damping parameter found in the literature. As the reduced damping parameter increases, lock-in becomes characterized by a decreasing peak structural amplitude (see, for example, Fig. 1 of Ref. [4]) and occurs over a decreasing band of velocities (see, for example, Fig. 4 of Ref. [5]). It is also worth noting that different phenomena are seen in structures with high and low structure–fluid density ratios $m^* = m/\rho D^2$, where m is the cylinder mass per unit length and ρ is the fluid density. For systems with high m^*, the vortex-shedding frequency is entrained by the structural frequency. For systems with low m^*, it is the fluid oscillation which sets the frequency and the entrainment frequency instead tends towards the shedding frequency f_v.

While resonance in flow-induced in-line oscillations of circular cylinders is an important topic, especially for systems with small structural damping (or small reduced damping parameters,

depending on the mass ratio), it is not considered as an independent topic in this review. Lock-in occurs when the in-line frequency approaches twice the Strouhal frequency (f_v) and the amplitude of the alternating force (drag fluctuations) and the response of the cylinder are an order of magnitude smaller than those in the transverse direction [2]. Defining the reduced velocity as $V_r = U/f_n D$, the most prominent feature of in-line oscillations of a rigid spring-mounted circular cylinder is the existence two excitation regions separated by $V_r \simeq 2$: symmetric vortex shedding for $V_r < 2$, and alternating vortex streets for $V_r > 2$ [6].

The engineering implications of VIV have been well documented in the literature. Structures such as tall buildings, chimneys, stacks and long-span bridges develop pronounced vibrations when exposed to fluid flow. See Refs. [7–10] for studies focusing on the VIV of these structures. The length and higher flexibility of some of these structures further aggravate the problem. In offshore applications, VIV of long slender structures such as pipelines, risers, tendons, and spar platforms challenge engineering designers [11]. Some examples of fundamental studies on the nature of the VIV of marine structures are included in Refs. [12–16]. Extensive research has also been done in the area of VIV assessment [17–19] and suppression [20,21].

In this review, both experimental and theoretical investigations of the fundamental aspects of vortex-induced vibration of circular cylinders are discussed in some detail. The authors' goal has been to be thorough without being exhaustive. The main focus of this review is on the semi-empirical models used to predict the response of the cylinder to the forces from the flow. These models are not rigorous and generally provide minimal insights into the flow field. To understand the flow effect on a structure, it is important that the actual flow field be described. Consequently, a secondary focus of this review is to discuss the flow characteristics around the cylinder. The flow field generated by flow separation around a body is a very complex fluid dynamics problem. However, much progress has been made toward the understanding of flow around bluff bodies. This is especially true in the field of computational fluid dynamics (CFD), and in keeping with the primary focus of this review, only selected papers highlighting this progress have been included.

While many reviews of the subject have been written in the past [2,5,22–25], a more contemporary review paper focusing on semi-empirical models is needed. The importance of such a paper follows from the fact that while VIV continues to be the subject of intensive research efforts and is quickly evolving, many of these simplified models continue to be used today. Among their attractions is the fact that they can be used in higher Reynolds number flows than CFD models and they have been solved in both the time and frequency domains. In addition, an alternative new method for the modelling of VIV is presented. The method is based on the variational principles of mechanics and leads to a more fundamental (without ad hoc assumptions) derivation of the equations of motion, yet remains inexorably linked to physical data. Experimental data help to verify the model predictions, thus leading to the most advantageous model framework.

2. Experimental studies

There are innumerable experimental studies on the vortex-induced vibration of bluff bodies, especially circular cylinders. These studies have examined a multitude of phenomena, from vortex

shedding from a stationary bluff body to vortex shedding from an elastic body. The vibration caused by vortices generated by the flow past a structure depends on several factors. The correlation of the force components, the shedding frequency, the Reynolds number, the material damping and structural stiffness of the cylinder, and the added mass effect are just a few of these. The literature is rich with experiments in which many of these factors have been considered, usually by varying one or two factors and holding the rest fixed. Here, key papers highlighting the influences of some of these factors on the structural response are discussed. Attention is focused mostly on results pertaining to the structural response. However, since VIV is indeed a coupled phenomena, some mention must be made of the hydrodynamics. Some factors that affect the cylinder response, such as the surface roughness of cylinder and turbulence (intensity and scale) in the incoming flow, are not considered here.

Before proceeding, it is worthwhile to define those variables that consistently appear in the equations developed in this section of the review. In this way, it will not be necessary to redefine them each time, unless introduction of a different notation is required. The outer diameter of a circular cylinder is designated by D, the length of the cylinder by L, the free-stream velocity of the flow by U, and the fluid density by ρ. The Strouhal number, S, is defined as $S = f_v D/U$, where f_v is taken to be the natural vortex-shedding frequency of a fixed cylinder. The reduced velocity is defined as $V_r = U/f_n D$, where f_n is the natural frequency of the structure. Due to discrepancies in the VIV literature as to how the natural frequency is defined, it will be defined on a case-by-case basis. The natural frequency is not the same in air as in water since the latter includes the effects of added mass. The normalized damping is defined as $\zeta = c_{\text{sys}}/c_{\text{crit}}$, where c_{sys} is the system damping, and c_{crit} is the critical damping.

Bearman [5] presents a comprehensive review of experimental studies related to vortex shedding from bluff bodies. He addresses the important question of the role of afterbody shape in vortex-induced vibration and results pertaining to a variety of afterbody shapes are included. Bearman first examines the mechanism of vortex shedding from a fixed bluff body. The presence of two shear layers is primarily responsible for vortex shedding. The presence of the body does not directly cause the vortex shedding, but it instead modifies the vortex-shedding process by allowing feedback between the wake and the shedding of circulation at the separation points.

Another important point discussed is the absence of two-dimensionality in the vortices shed from a two-dimensional bluff body in uniform flow. The spanwise coupling between the two shear layers that leads to generation of vortex shedding is generally weak. This implies that unsteady quantities related to vortex shedding (e.g., surface pressure) are not constant along the span of the body. However, continuous regions of similar properties are characterized in terms of correlation lengths. Small departures from two-dimensionality, in the form of a taper along the axis of the bluff body or the presence of shear flow, leads to significant reductions in the vortex-shedding correlation length.

Bearman also examines vortex shedding from oscillating bluff bodies. The fundamental difference between fixed and oscillating bluff bodies is that the motion of the cylinder can take control of the instability mechanism that leads to vortex-shedding. This is manifested in the capture of the vortex-shedding frequency by the body natural frequency over a range of reduced velocities. The vortex-shedding correlation length is significantly increased when the vortex-shedding frequency coincides with the body oscillation frequency. The range of reduced velocities over which the vortex-shedding frequency coincides with the natural frequency of the body

depends on the oscillation amplitude. Larger ranges of frequency capture result from larger oscillation amplitudes.

It is worth pointing out that the capture range will always include the reduced velocity value corresponding to the inverse Strouhal number, and that maximum amplitude is attained near to (but not exactly) this value. In other words, the reduced velocity for maximum amplitude is close to $1/S$. The location of this resonant point within the capture range depends on the shape of the afterbody.

In the capture range, flow conditions around a bluff body change rapidly. The fluctuating lift coefficient increases due to the improved two-dimensionality of the flow. This improved two-dimensionality (increased correlation length) increases the strength of the shed vortices. The increase in the lift coefficient can also be attributed to the influence of the body motion, which manifests itself through the reduction of the length of the vortex-formation region and the formation of stronger vortices near the base of the body. The mechanism governing the phase of the vortex-induced force relative to the body motion has also been explored by Bearman. The changes in phase angle through the capture range occur in a progressive and not discontinuous fashion. In the lower end of the lock-in range, a vortex formed on one side of the cylinder is shed when the cylinder is near to attaining its maximum amplitude on the opposite side (mode 1). As the reduced velocity is increased, the timing of vortex shedding suddenly changes, and the same vortex is now shed when the cylinder reaches its maximum amplitude on the same side (mode 2). Clearly, the point in an oscillation cycle at which the cylinder receives its maximum transverse thrust changes drastically over a narrow range of reduced velocities. Zdravkovich [26] discusses in detail the modification of vortex shedding in the synchronization range. The existence of the two modes, modes 1 and 2, is used to explain the existence of the hysteresis effect.

Bearman [5] discusses free vs. forced vibrations in experiments. Forced vibration experiments offer the advantage that the reduced velocity and amplitude ratios can be independently varied. In free vibration experiments, these two parameters are inseparable, since varying the reduced velocity leads to changes in the amplitude ratio. The major disadvantage of forced vibration experiments is that only a very limited range of reduced velocities and amplitude ratios studied will actually correspond to those encountered in a free vibration. Bearman states that free and forced vibration flows are the same, provided that one assumes that the exact history of motion is inconsequential.

2.1. Fluid forces on an oscillating cylinder

Vortex-shedding from a circular cylinder produces alternating forces on the cylinder and it is these forces which cause the cylinder to vibrate if it is free to do so. Experiments by Sarpkaya [27] determine the in-phase and out-of-phase components of the time-dependent force acting on a rigid circular cylinder undergoing forced transverse oscillations in a uniform stream. These force components are used in the prediction of the dynamic response of an elastically mounted cylinder in the synchronization range. The details of this aspect of the investigation are relegated to the section of this review describing semi-empirical models. Preliminary experimental work measures the mean fluid-induced force on the cylinder in the direction of flow for various amplitudes and frequencies of cylinder oscillation in the transverse direction. The in-line force is found to increase as A/D increases, where A is the transverse oscillation amplitude. For a given value of A/D, the

in-line force reaches a maximum for $D/\bar{V}T$ (mathematically similar to a Strouhal number) in the range 0.18–0.20, where T is the oscillation period and $\bar{V}$ has the same meaning as U. Furthermore, synchronization is found to occur at a frequency slightly lower than the Strouhal frequency for a stationary cylinder, 0.21, corresponding to the range of Reynolds numbers considered by Sarpkaya, 5000–25,000.

In considering the transverse force on the cylinder, the lift coefficient C_L is expressed in terms of an in-phase inertia force and an out-of-phase drag force. The inertia coefficient C_{ml} characterizes the in-phase force, while the out-of-phase force is characterized by the drag coefficient C_{dl}. The drag and inertia coefficients are assumed independent of the Reynolds number in the range considered, 5000–25,000. Synchronization is manifested by a rapid decrease in the inertia coefficient and a rapid increase in the absolute value of the drag coefficient. The experiments also confirm that the net effect of the cylinder–flow interaction near synchronization, for $A/D < 1$, is the same as for periodic flow over a cylinder at rest. This suggests that the fluid becomes the oscillator under these conditions.

The major implication is then that use of the maximum inertia coefficient obtained by oscillating the cylinder in a fluid otherwise at rest, $C_{ml} = 1$, does not give the correct results since C_{ml} has been shown to reach a value of about 2 near synchronization. There is a range of $V_r = \bar{V}T/D$ near perfect synchronization ($V_r \approx 5$), where the drag coefficient is found to be in-phase (negative) with the direction of motion of the cylinder. In this range, the drag coefficient actually helps to magnify the oscillations, and for this reason the range is often referred to as the negative damping region.

Gopalkrishnan [28] measures the vortex-induced lift and drag forces on a smooth circular cylinder undergoing forced sinusoidal oscillations transverse to the free-stream. The measurements are conducted in water. The lift force phase angle (defined in the same way as ϕ° in Fig. 1) is found to be very different for large oscillation amplitudes than for small oscillation amplitudes. This is partially responsible for the amplitude-limited nature of VIV. The range of reduced velocities where the cylinder is excited into oscillations by the flow (the lift coefficient excitation region) is found to not coincide with the lock-in region. Furthermore, the excitation region is found to be dependent on the phase, while lock-in is found to be a frequency-dependent effect. The author also measures the lift and drag forces on a cylinder subjected to an amplitude-modulated force causing beating motions. The presence of beating is found to cause a reduction in the mean drag coefficient, an increase in the rms oscillating drag coefficient, and increased extent of the primary excitation regions (vs. sinusoidal excitation). The overall magnitude of the lift coefficient was comparable to that corresponding to sinusoidal forcing.

2.2. Three-dimensionality and free-surface effects

Three-dimensional features naturally arise in the VIV problem as the real domain is considered as spanwise extended: elastic structures are characterized by their eigenmodes and wake flows show secondary instabilities [29]. The transition to three-dimensionality in the near wake of a circular cylinder is discussed by Williamson [30]. Three-dimensional structures in the wake were found to occur for Reynolds numbers greater than about 178. These three-dimensional structures are attributed directly to the deformation of the primary wake vortices, and were not the result of any secondary (Kelvin–Helmholtz) vortices caused by high-frequency oscillations within the

separating shear layers. The transition to three-dimensionality is found to involve two successive transitions, each characterized by a discontinuity in the Strouhal–Reynolds number relationship. These discontinuities can be seen in Fig. 2. The first discontinuity (*Re*: 170–180) is associated with the transition from periodic and laminar vortex shedding to shedding involving the formation of vortex loops. The second discontinuity (*Re*: 225–270) is related to the transition from the vortex loops to finer-scale streamwise vortices. The first discontinuity is found to be hysteretic, while the second discontinuity is not.

A more comprehensive discussion on these discontinuities (so-called mode A and mode B secondary 3-D instabilities) and vortex dynamics in bluff body wakes in general can be found in two review papers by Williamson [31,32]. Specifically, comparisons of measurements and theoretical predictions of spanwise instabilities for modes "A" and "B" are given in Fig. 10 of Williamson [32].

The question of three-dimensionality in the wake of a surface-piercing rigid cylinder mounted as an inverted pendulum is examined in detail by Voorhees and Wei [33]. The cylinder is characterized by a low mass ratio, $m^* = 1.90$, and high mass damping, $m^*\zeta = 0.103$. The mass ratio is defined as the mass of the cylinder assembly divided by the mass of water displaced by the cylinder, $m^* = 4m/\rho\pi D^2 L$. The ratio of mechanical (in air) to critical damping is represented by ζ. The critical damping is defined as $c_{\text{crit}} = 2\sqrt{k(m + m_a)}$, where m_a is the added mass. This study, for *Re*: 2300–6800, found that the response characteristics of the cylinder are similar to those seen in elastically mounted cylinders of similar m^* and $m^*\zeta$. Strong axial flows associated with the Kármán vortices are observed, and these flows are generally directed upwards towards the free surface. Below the free surface, these axial flows can be predominantly attributed to the linearly increasing oscillation amplitude along the span. Near the free surface, however, there is an equal probability of upflow and downflow. These upflows and downflows are shown to be well correlated to the quasi-periodic beating of the cylinder amplitude at the reference reduced velocity $U^* = 4.9$ (*Re*: 3400) in the synchronization range. The reduced velocity U^* has the same meaning as V_r and is defined using the natural frequency of the structure in still water. In essence, the effect

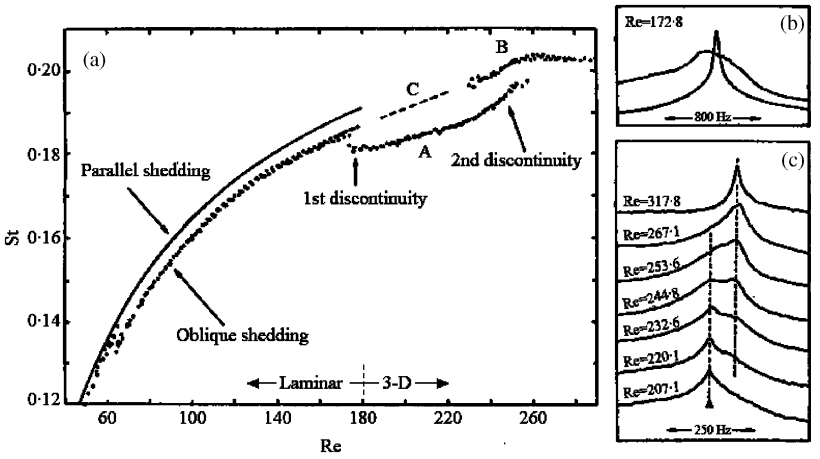

Fig. 2. (a) Variation in Strouhal number as a function of Reynolds number; (b) frequency spectra at first discontinuity; (c) frequency spectra at second discontinuity [39].

of the free surface is to disrupt the primary upflow mechanism and also to induce lateral spreading of the top portions of the Kármán vortices.

Regarding free surfaces, several fundamental aspects of vortex formation are found to depend on the gap between the cylinder and the free surface, as discussed by Lin and Rockwell [34] for the case of a fully submerged cylinder oriented parallel to the free surface. The influence of a free surface on the wake structure has also been investigated by Sheridan et al. [35–37].

2.3. Vortex-shedding modes and synchronization regions

The character of the vortex shedding is important in that it influences the phase of lift force and, consequently, the energy transfer between the fluid and the body. Williamson and Roshko [38] explore the existence of regions of vortex synchronization in the wavelength–amplitude plane. From the outset, the Reynolds number is not treated as an independent parameter in this study. The Reynolds number is kept within a certain range, $300 < Re < 1000$, but is never held fixed. The amplitude ratio equals A/D. The wavelength ratio is $\lambda/D = UT_e/D$, where $T_e = 1/f_e$ is the period of cylinder oscillation in the transverse direction. The wavelength ratio is equivalent to the reduced velocity, but has the distinct advantage that it introduces the trajectory along which the body travels relative to the fluid.

Within the fundamental lock-in region ($\lambda/D \approx 5$ or $T_e \approx T_s$, where T_s is the period of vortex shedding for a non-oscillating cylinder), the acceleration of the cylinder at the start of each half-cycle induces the rolling up of each of the separating shear layers into a new pair of vortices. Consequently, the cylinder sheds four regions of vorticity in each cycle. The authors find that, below a critical trajectory wavelength (for a given amplitude ratio), each half-cycle results in the coalescence of a pair like-signed vortices. Consequently, two regions of opposite vorticity are fed into the downstream wake per cycle. The resulting formation is similar to the classic von Kármán vortex street wake and is called the 2S mode. Above the critical trajectory wavelength, the like-sign vortices are found to convect away from each other. Each of these vortices then paired up with a vortex of opposite sign. The resulting formation is two vortex pairs (of opposite signs) convecting laterally away from the centerline. This mode is called the 2P mode.

At exactly the critical wavelength, four regions are no longer formed. Only two vortices are formed in each cycle, and the resulting shed vorticity is more concentrated than at other wavelengths. This condition is called the resonant synchronization. The resonant synchronization is important because it coincides (approximately) with the peak in the lift forces seen in experimental results. The conclusion is that the larger forces are being induced by the shedding of more concentrated vorticity. Fig. 3 is a map of vortex synchronization patterns near the fundamental lock-in region.

The transition from the 2S mode to the 2P mode can be sudden, and it is this abrupt change in the dynamics of the vortex wake that is a plausible explanation for the sharp changes in the character of the body forces through the primary lock-in. The jump in the phase angle ϕ between the lift force and the body motion seen near the natural shedding frequency ($T_e \approx T_s$) can be attributed to the process of pairing in the 2P mode, which causes a sharp change in the timing of the shedding. Since it is possible that in a certain small range of wavelength either one of the two modes can exist, hysteresis will result. The 2P $\rightarrow$2S (decreasing wavelength) jump occurs for a

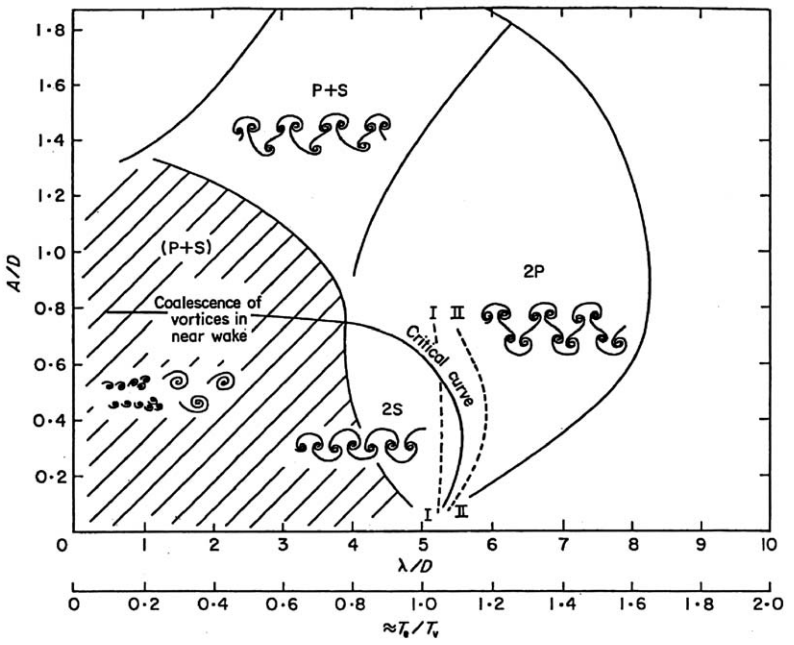

Fig. 3. Map of vortex synchronization near the fundamental lock-in. A/D is the amplitude ratio and λ/D is the wavelength ratio. The "critical curve" represents the transition from one mode of vortex formation to another. Curves I and II represent locations where the forces on the body show a sharp jump [38].

lower wavelength than does the 2S → 2P (increasing wavelength) jump. This is illustrated in Fig. 4.

A more general approach for categorizing the vortex-shedding modes is taken by Zdravkovich [39]. Vortex shedding from a cylinder is classified as either low-speed mode or high-speed mode. The low-speed mode is related to laminar wake instability, while the high-speed mode is related to vortex formation and shedding. The transition state between the low- and high-speed modes is characterized by "fingers" or distortions of eddy filaments in the near wake. These "fingers" cause irregular vortex filaments to appear along the span. Zdravkovich also describes two modes in the streamwise oscillation of a cylinder in an oscillatory flow. Near the synchronization frequency, which would in this case be approximately twice the natural shedding frequency, the following modes are found: one vortex formed per half-cycle and two vortices formed per half-cycle. Interestingly, the transition state from the first mode to the second mode is characterized by one vortex formed in odd half-cycles and two vortices formed in even half-cycles.

2.4. The frequency dependence of the added mass

The added mass is not the same for a body oscillating at a given frequency in a still fluid as for a body oscillating at the same frequency in a moving fluid. The relationship between added mass and response frequency for a lightly damped elastically mounted rigid cylinder in uniform flow (Re: $10^4-6\times10^4$) is examined by Vikestad et al. [40]. The cylinder is characterized by a low mass ratio $m^* = m/\rho D^2 = 1.3$. The cylinder is allowed to vibrate in the crossflow direction only. Two

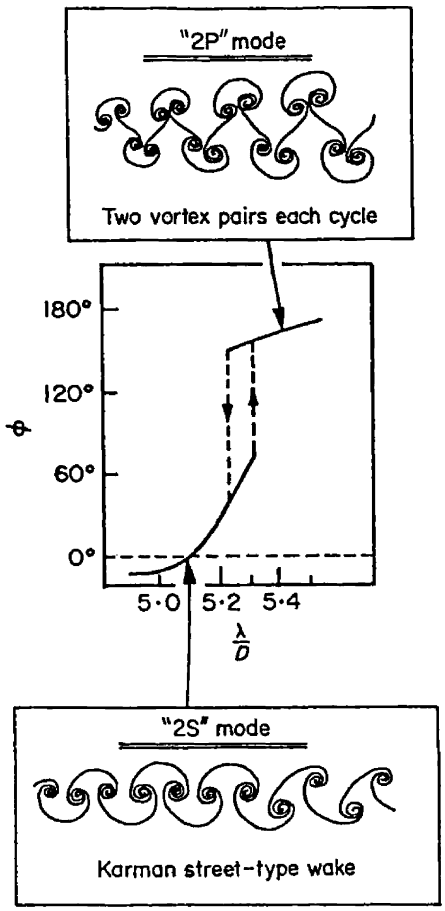

Fig. 4. Variation of the lift force phase angle ϕ with wavelength ratio λ/D [38].

different experiments are conducted for various values of the reduced velocity: those with no support excitation, and those with support (external) excitation at a given frequency. The reduced velocity $U_r = U/f_0 D$ is defined on the basis of the natural frequency (f_0) measured in still water ($C_a = 1.04$). Since the natural frequency is generally not constant but depends on the added mass ($f_n = f_n(C_a)$), it is not possible to conduct experiments on the dependence of the oscillation frequency on the added mass without fixing the reduced velocity. This follows from the fact that the oscillation frequency is itself dependent on the reduced velocity, leading to a "circular" problem. The added mass coefficient is estimated from

$$C_a = -\frac{8}{nT\rho\pi D^2 L(\omega^2 x_0)^2}\int_t^{t+nT} F_v \ddot{x}\,\mathrm{d}t, \tag{1}$$

where F_v is the crossflow component of the total hydrodynamic force (minus the cylinder inertia force), $\ddot{x}$ is the cylinder acceleration, T is the period of cylinder oscillation, $\omega^2 x_0$ is the acceleration amplitude and n is the number of periods over which integration is performed.

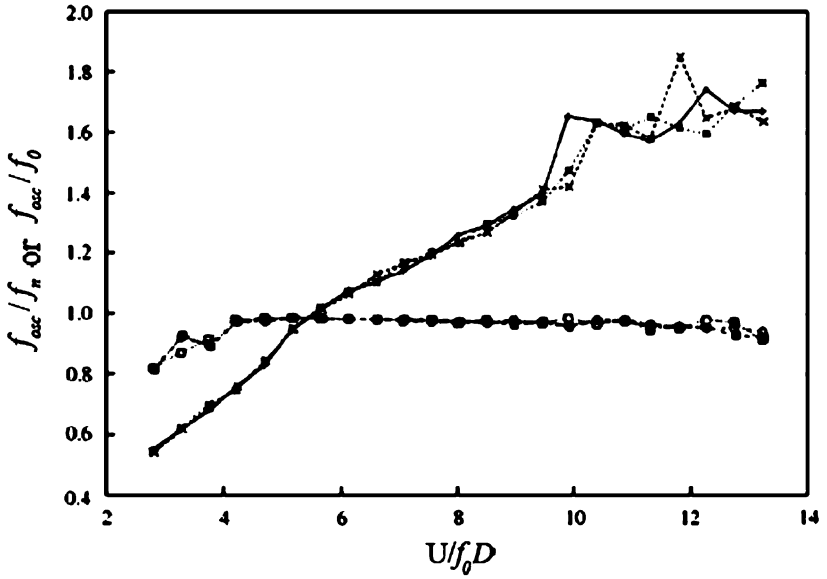

Fig. 5. Mean oscillation frequency divided by the natural frequency in still water, f_{osc}/f_0, shown by the sloped lines. Mean oscillation frequency divided by the true natural frequency, f_{osc}/f_n, shown by the horizontal lines. Both are shown as functions of the reduced velocity U_r [40].

For experiments conducted without support excitation, two different calculations are performed using Eq. (1): an average C_a over many periods, and a time-dependent C_a obtained by averaging over a sequence of single periods. For C_a calculated over many periods, the authors define the mean oscillation frequency as $f_{\mathrm{osc}} = \sqrt{(\ddot{x}_{\mathrm{rms}}/x_{\mathrm{rms}})}/2\pi$ and the true natural frequency as

$$f_n(U_r) = \frac{1}{2\pi}\sqrt{\frac{k_{\mathrm{TOT}}}{m + \rho V_{\mathrm{cyl}} C_a(U_r)}},$$

where m is the cylinder effective dry mass, k_{TOT} is the total stiffness of the oscillatory system, and V_{cyl} is the cylinder volume. The results of plotting f_{osc}/f_0 and f_{osc}/f_n vs. U_r (Fig. 5) show no evidence that the oscillation frequency is locked-in to one fixed natural frequency. Instead, the oscillation frequency is the true natural frequency over a wide range of reduced velocities. In fact, since the added mass coefficient decreases with reduced velocity (see Fig. 4(a) of Ref. [40]), the natural frequency increases (Eq. (1)) with reduced velocity. According to the authors, this is the reason why low mass ratio cylinders have lock-in regions that extend over a broader range of flow speeds. Cylinders with high mass ratios show smaller increases in natural frequency with variations in added mass. The mass ratio dependence of the added mass effect has also been described by Khalak and Williamson [4].

For C_a calculated over single periods, the variation in the added mass from one vibration cycle to next is shown to be considerably large. This variation is found to be least in the range of reduced velocities U_r: 4–6. This is the range of reduced velocities for which there is strong correlation between the added mass coefficient and the cylinder displacement. The variation in the

added mass from cycle to cycle is also shown to be closely correlated to the cycle-to-cycle variation in the response frequency. Again, this is attributed to changes in the added mass-dependent natural frequency. The interested reader is referred to the journal paper for details of the experimental results pertaining to support (external) excitation.

2.5. Dynamics of cylinders with low mass damping

Khalak and Williamson [41] study the forces and vortex-induced response of a rigid circular cylinder in an experimental facility characterized by a very low mass ratio m^* and a very low normalized damping ratio ζ. The mass ratio and critical damping are defined as $m^* = 4m/\rho D^2 L$ and $c_{\text{crit}} = \sqrt{k(m+m_a)}$, respectively. The added mass m_a is taken to be equal to the displaced mass of the fluid (the potential added mass coefficient C_A is assumed to have a value of unity). The combined mass-damping parameter $m^*\zeta$ has a value of 0.013, a value at least one order of magnitude lower than any previous study. Initially, the cylinder is held fixed (static) in a uniform flow. The test cylinder has either a free end, which produced oblique vortex shedding, or an end cylinder (a larger cylinder placed coaxially), which produces parallel shedding. The total fluctuating lift and drag forces on the cylinder are measured for both end conditions as a function of the Reynolds number. The time-averaged drag coefficient is found to be consistently higher in the case of parallel shedding and this result is essentially independent of Reynold number. The rms lift coefficient is also found to be higher in the case of parallel shedding, but the difference is not Reynolds number independent. Spectral analysis indicates that the lift force is dominated by a single peak at the shedding frequency in the case of parallel shedding, while in the case of oblique shedding two smaller peaks are present.

The transverse response of the elastically mounted cylinder is also examined in the same work. The response of the cylinder is found to have two distinct resonant branches. Hysteresis results from moving between these branches and the jump between the branches can be interpreted as a change in the vortex-shedding mode. These two resonant branches, called the upper (very high amplitude response) and lower branches (moderate amplitude response), can be seen in Fig. 6. Note that the reduced velocity is formed using the natural frequency in still water f_n, $U^* = U/f_n D$. Also shown is data from Feng [42] , which is obtained for a much higher mass-damping parameter of $m^*\zeta = 0.36$. Clearly, there is a substantial increase in both the amplitude and range of the response for lower values of mass damping. Note that the values of m^* and ζ did not include the effects of added mass. Also shown in Fig. 6 are the initial excitation region and the desynchronization region as described in Ref. [43]. The classical experiments of Feng (high $m^*\zeta$) show the absence of the upper branch and only two response branches exist. The initial branch has been shown to be associated with the 2S mode of vortex formation, while the lower branch corresponds with the 2P mode [4].

The mass ratio m^* and the normalized damping ζ are found to independently affect the response of the system. By maintaining the value of $m^*\zeta$ constant, the value of m^* is independently adjusted. Lower values of m^* are manifested in the form of higher response amplitudes and a larger range of response in the lower resonance branch. However, changes to m^* do not significantly alter the characteristics of the upper branch. The level of maximum excitation in the upper branch is found to be well characterized by the combined mass-damping parameter $m^*\zeta$

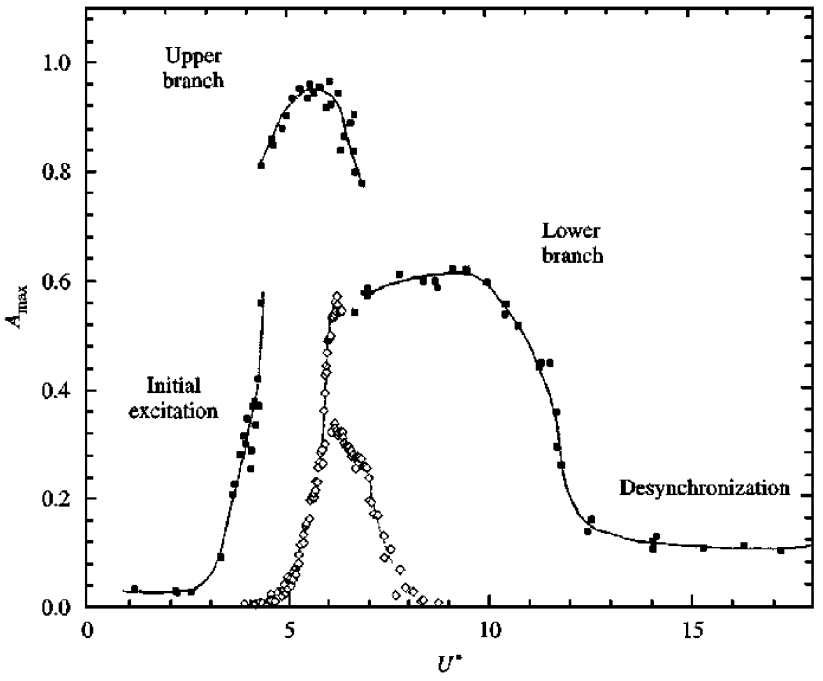

Fig. 6. Maximum response amplitudes A_{max} as functions of the reduced velocity U^* for $m^* = 2.4$ (■) and $m^* = 248$ (◇) [41].

[44,4]. Most importantly, these effects cannot be explained by including the added mass. Presumably, for low mass ratios the inertia of the fluid being accelerated by the cylinder is important. A linear equation of motion is developed, with the inclusion of an inviscid added-mass force. The failure of the added mass to explain the mass dependence of the response led the authors to conjecture that it is instead the phase angle ϕ which is responsible. The classical "mass-damping" parameter $(m^* + C_A)\zeta$ has been shown to collapse peak amplitude data over a wide range of mass ratios. The use of the combined parameter is valid down to atleast $(m^* + C_A)\zeta \sim 0.006$ [4].

In a subsequent paper [43], Khalak and Williamson show that as the normalized velocity is increased, the transition from the initial excitation region to the upper branch is hysteretic. The transition from the upper branch to the lower branch also involves a jump, but is followed by intermittent switching. This intermittence is clearly seen in the instantaneous phase measurements between the lift force and the displacement in the transition region. Both of the transitions are associated with jumps in response amplitude and frequency, but only the transition from the upper to the lower branch is associated with a 180° jump in the phase angle. Fig. 7 is a schematic of the differences between high-$m^*\zeta$ and low-$m^*\zeta$ amplitude response.

Perhaps the most interesting result is that, in the synchronization regime, the frequency of cylinder oscillation is significantly higher than the structural natural frequency. In other words, $f^* = f_0/f_n > 1$ through the synchronization regime. Yet, f_0 also remains below the natural vortex-shedding frequency of a non-oscillating cylinder in this regime (see Fig. 4 of Ref. [4]).

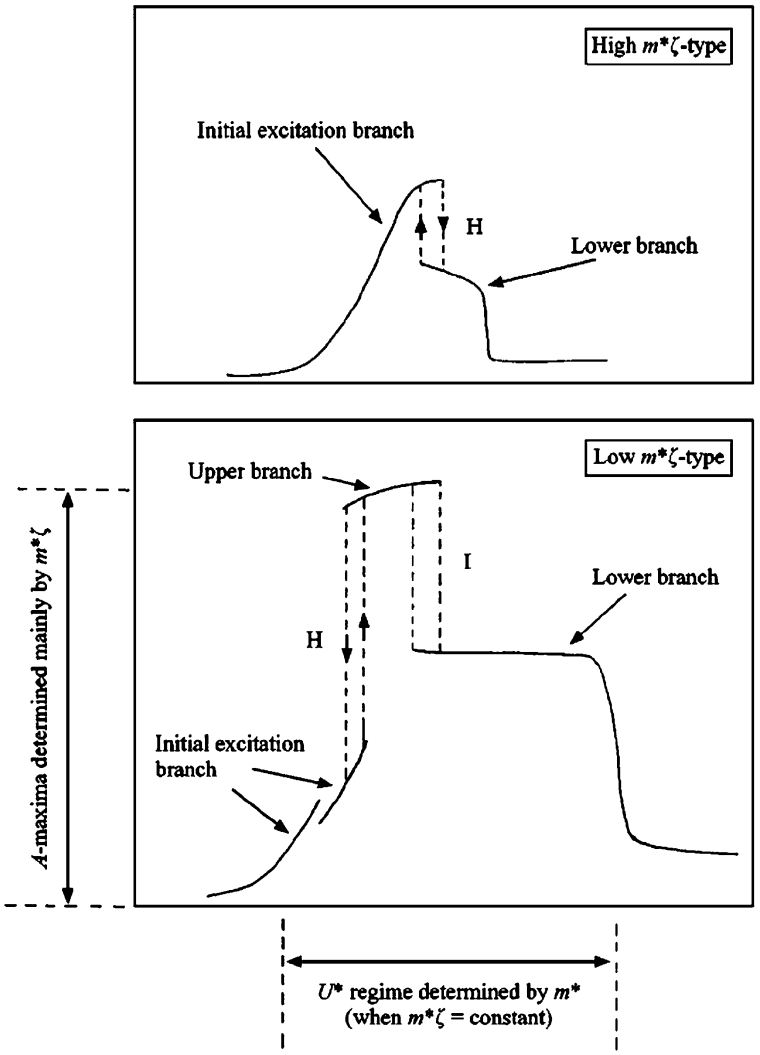

Fig. 7. The two distinct types of amplitude response: high $m^*\zeta$ and low $m^*\zeta$. The mode transitions are either hysteretic (H) or intermittently switching (I) [4].

Synchronization, as used here, is defined as the matching of the frequency of the periodic wake vortex mode with the cylinder oscillation frequency. The departure of f^* from unity is not what would be expected from a classical lock-in. The major implication is that for cylinders with low mass ratios, it is not possible to define lock-in as a matching (or more correctly, a near matching) of the shedding frequency and the still water natural frequency, $f^* \approx 1$. Other investigations by Williamson's group at Cornell can be found in Refs. [45–47].

As part of a new paradigm to support the reduced-order analytical modeling of fluid–structure interactions, Dong et al. [48] use high-resolution digital particle image velocimetry (DPIV) to

measure fluid energy transport terms. The terms form part of the equation of motion for a rigid circular cylinder with a low mass damping ($m^*\zeta = 0.0377$) mounted like an inverted pendulum. The equation of motion is derived using a form of Hamilton's principle appropriately developed for systems of changing mass. More specifically, the governing equation is formulated using the control volume (CV) approach. Further details of this approach will be outlined in Section 3.4. It is worth mentioning here that, except for the quasi-two-dimensionality of the flow, no empirical assumptions are incorporated into the model. The assumption made is reasonable in light of the fact that Voorhees and Wei [33] show that three-dimensional effects are dominant near the free surface. The fluid energy terms which are calculated from the DPIV velocity vectors are the time rate change of the fluid kinetic energy within the CV, the net flux of fluid kinetic energy across the boundaries of the CV, and the work done on the CV boundaries by pressure and viscous forces. These terms are calculated for a single value of the reduced velocity U^* corresponding to a Reynolds number of 2300. This corresponds to the resonant synchronization regime where the cylinder response exhibits a beating behavior (i.e., large amplitude-modulated oscillations).

The results of the study indicate that the choice of a CV is crucial to obtaining energy transport traces that are more easily interpreted.

3. Semi-empirical models

In this review, every attempt has been made to preserve the notation of the governing equations as given in the references. This facilitates the reader's ability to correspond between this review and a given paper. Work with structures undergoing vortex-induced vibration can be classified into three main types. The first class consists of wake–body (wake–oscillator) coupled models, in which the body and the wake oscillations are coupled through common terms in equations for both. The second class, the single degree-of-freedom (sdof) models, use a single dynamic equation with aeroelastic forcing terms on the right-hand side of the equation. The third class, the force–decomposition models, rely on measurement of certain components of the forces on the structure from experiments.

3.1. Wake–oscillator models

Several wake–oscillator models have been proposed in the literature. The models generally have the following characteristics: The oscillator is self-exciting and self-limiting, the natural frequency of the oscillator is proportional to the free stream velocity such that the Strouhal relationship is satisfied, and the cylinder motion interacts with the oscillator. The latter essentially says that the motion of the cylinder strongly affects the lift forces, which in turn influences the cylinder motion. Also, the models assume that the flow around the cylinder is two-dimensional (i.e., the flow is fully correlated). Consequently, the models are limited to moderate to large response amplitudes. These models often do not include any analysis of the flow field and their value is at best to explain and simulate experimental results. For this reason, these models are often referred to as *phenomenological*. The modeler's desire is to obtain the equations of the cylinder oscillator and the fluid oscillator by independent means and then use them together to predict the response of

the combined fluid–elastic system [49]. Parkinson [50] presents a comprehensive review of the modeling of flow-induced vibrations in bluff bodies.

3.1.1. Rigid cylinders

Bishop and Hassan [51] are credited with first suggesting the idea of using a van der Pol type oscillator to represent the time-varying forces on a cylinder due to vortex shedding. Hartlen and Currie [52] formulate the most noteworthy of the oscillator models. In their model, a van der Pol soft nonlinear oscillator for the lift force is coupled to the cylinder motion by a linear dependence on the cylinder velocity. The cylinder motion is restricted to pure translation in the transverse direction, perpendicular to both the flow direction and the cylinder axis. The cylinder is restrained by linear springs and is linearly damped. The model is given by the pair of coupled non-dimensional differential equations,

$$x_r'' + 2\zeta x_r' + x_r = a\omega_0^2 c_L, \tag{2}$$

$$c_L'' - \alpha\omega_0 c_L' + \frac{\gamma}{\omega_0}(c_L')^3 + \omega_0^2 c_L = b x_r', \tag{3}$$

where primes denote time derivatives with respect to the non-dimensional time $\tau = \omega_n t$, x_r is the dimensionless cylinder displacement, c_L is the lift coefficient, ω_0 is the ratio of the Strouhal shedding frequency and the natural frequency of the cylinder, $\omega_0 = f_0/f_n$, and ζ is the material damping factor. The parameter a is a known dimensionless constant. Of the undetermined parameters α, γ, and b, only two must be chosen to provide the best fit to experimental data. This follows from the fact that α and γ are related to each other by the expression $C_{L_0} = (4\alpha/3\gamma)^{1/2}$, where C_{L_0} is the amplitude of the fluctuation of c_L on a fixed cylinder. It is worth noting that the second term on the left-hand side of Eq. (3) provides the growth of the lift coefficient c_L, while the third term on the left-hand side of the same equation prevents its unlimited growth. These terms are important to the success of the model because the large-amplitude oscillations characteristic of VIV are accompanied by a significant (yet finite) increase in the lift coefficient.

With the appropriate choice of parameters, the Hartlen and Currie model qualitatively captures many of the features seen in experimental results [53,2]. For instance, a large cylinder-oscillation amplitude resonance region occurs when the vortex-shedding frequency is near the natural frequency of the cylinder. The frequency of oscillation in this region is nearly constant at a value close to the cylinder natural frequency. The hysteresis effects seen in the experimental results of Feng [42] are also seen in the analysis of the Hartlen and Currie model by Ng et al. [53] using multiple scales and bifurcation analyses. Fig. 8 is an illustration of the amplitude and frequency responses of the Hartlen and Currie model with $\zeta = 0.0015$, $\alpha = 0.02$, $\gamma = 2/3$, $a = 0.002$ and $b = 0.4$. It is evident that much of the lock-in domain is characterized by hysteresis and that there is asymmetry in the amplitude response. These features are a direct result of the velocity coupling term bx_r' used in Eq. (3).

Skop and Griffin [54] develop a model to resolve what they feel are inadequacies of the Hartlen and Currie model, including the fact that the model parameters are not related to any physical parameters of the system. A modified van der Pol equation is again employed as the governing equation of the lift, and an equation is presented for the oscillatory motion of the body. The

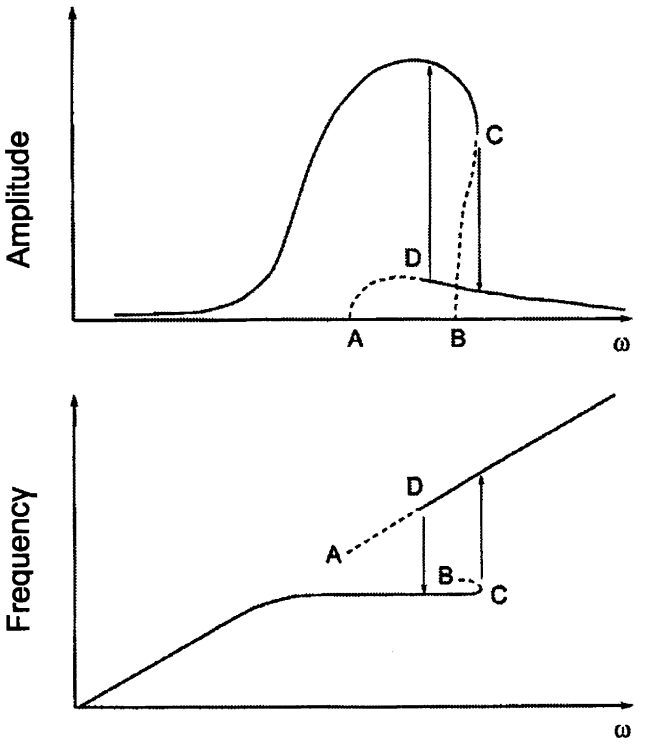

Fig. 8. Amplitude and frequency response of the Hartlen–Currie model. ω is proportional to the flow velocity. Solid lines represent stable branches of the periodic motions, while dotted lines represent unstable branches. Arrows show jumps in amplitude and frequency corresponding to sweeps of ω [53].

equations are

$$\frac{\ddot{X}}{D} + 2\zeta\omega_n \frac{\dot{X}}{D} + \omega_n^2 \frac{X}{D} = (\rho V^2 L/2M) C_L = \mu\omega_s^2 C_L, \tag{4}$$

$$\ddot{C}_L - \omega_s G\left[C_{L_0}^2 - \frac{4}{3}\left(\frac{\dot{C}_L}{\omega_s}\right)^2\right]\dot{C}_L + \omega_s^2\left[1 - \tfrac{4}{3}H\dot{C}_L^2\right]C_L = \omega_s F\left(\frac{\dot{X}}{D}\right), \tag{5}$$

where ω_s is the shedding frequency, C_L is the oscillating lift coefficient, C_{L_0} is the fluctuating lift amplitude from a stationary cylinder, ω_n is the undamped natural frequency of the spring–mass system, and ζ is the sum of the structural, fluid, and externally applied damping. M is the mass of the cylinder and $\mu = \rho LD^2/8\pi^2 S^2 M$ is a parameter representing the ratio of the displaced mass of fluid to the mass of the cylinder. The parameters G, H, and F are to be determined from experimental data.

Solutions to these governing equations in the lock-in state (frequency entrainment) are sought using the method of van der Pol, in which one seeks solutions of the form $X/D = aC_{L_0}\sin\omega t$ and $C_L = AC_{L_0}\sin(\omega t + \varphi)$, where φ is the phase difference between the fluctuating lift coefficient and

the cylinder displacement. Substitution of the assumed solutions into the governing equations results in relationships between the various model parameters. Relationships between the two independent model parameters G and H and the physical mass and damping parameters μ and ζ are formulated by considering a variety of experimental results from the literature and then using a best-fit line. For instance, the relation for G is given as $\log_{10} G = 0.23 - 0.19(\zeta/\mu)$. However, the fact that the parameters G and H are obtained at each experimental value of ζ and μ by trial and error is an inherent flaw in this model. The value of the third empirical constant is given as $F = 4G\zeta^2\mu H$.

Using these relationships, the authors are able to quantitatively predict the results of a different set of resonant vibration experiments found in the literature with reasonable accuracy. The question can, of course, be raised as to how much predictive value to assign a model which has been "tweaked" from the beginning.

In a subsequent paper, Griffin et al. [55] compare the results of their own experiments with spring-mounted cylinders in a wind tunnel and the results predicted by their wake oscillator model. Measurements are made of the vibration amplitude and frequency under a variety of flow conditions at Reynolds numbers between 350 and 1000. All measurements are conducted under conditions of synchronization between the vortex-shedding frequency and the cylinder oscillation frequency. The major conclusions of the study are as follows, with (E) denoting experimental results, (T) denoting theoretical results and (E–T) denoting compared results:

- The magnitude and location of the peak resonant amplitude and the detuning between the vibration and cylinder natural frequencies are quantitatively predicted by the model (E–T).
- The maximum lift occurs at a flow speed somewhat less than that which produces the largest amplitude (T).
- The maximum energy transfer to the cylinder occurs at the flow speed which produces the largest amplitude (E–T).
- There is a substantial change in the phase angle φ between lift and the cylinder motion in the synchronization regime (T).
- The energy transfer to the cylinder per vibration cycle will be positive if the lift force includes a component which is in phase with the cylinder velocity (T).
- Up to a 75% increase in the drag coefficient from the fixed cylinder value is measured at a peak amplitude of one diameter (E).

Like the Hartlen and Currie model, the Skop and Griffin model [54] contradicts several findings by Feng [42]. Feng finds that the maximum lift and maximum cylinder displacement occurred at the same value of flow speed. Feng also finds that the cylinder will continue to oscillate at its natural frequency outside the lock-in range.

Iwan and Blevins [56] arrive at fluid oscillator equations by considering the fluid mechanics of the vortex street. The model is based on the introduction of a hidden fluid variable z, which captures the fluid dynamics effects of the problem. The equations are

$$\ddot{y} + 2\zeta_T \omega_n \dot{y} + \omega_n^2 y = a_1' \ddot{z} + a_4'' \dot{z}\,\frac{U}{D}, \tag{6}$$

$$\ddot{z} + K'\frac{u_t}{D}\omega_s z = (a_1' - a_4')\,\frac{U}{D}\,\dot{z} - a_2'\,\frac{\dot{z}^3}{UD} + a_3'\ddot{y} + a_4'\,\frac{U}{D}\dot{y}, \tag{7}$$

where ζ_T is the total effective damping coefficient, u_t is the translational velocity of the vortex street shed from the cylinder, and K' is a parameter related to the Strouhal number and the ratio u_t/U. The total effective damping coefficient is the sum of the structural viscous damping and the viscous fluid damping. All of the empirical parameters a_i' and a_i'' of the model but one are determined from experimental data for fixed and harmonically forced cylinders. The model is then used to predict the response of elastically mounted rigid cylinders.

The response of the cylinder is found to be dependent on the structural viscous damping ζ_s, the ratio of the shedding frequency to the natural frequency of the cylinder ω_s/ω_n, and the ratio of the displaced fluid mass to the cylinder mass. This mass ratio is defined as $\rho D^2/2m$. The peak amplitude of cylinder oscillation for the resonant condition is found to depend on a single variable called the reduced mass-damping parameter, $\delta_r = 4\pi m\zeta_s/\rho D^2$. Note that this reduced mass-damping parameter is identical to the Scruton number mentioned in Section 1. The model correctly predicts the entrainment effect (or lock-in). The entrainment effect (width of the frequency band over which lock-in persists) is shown to increase with decreased structural damping, and increased ratio of displaced fluid mass to cylinder mass. The amplitude of the peak resonant response is found to be inversely proportional to the reduced damping.

Landl [57] includes a nonlinear aerodynamic damping term of fifth order in his two-equation model for vortex-induced vibrations of a bluff body. The equations are given in dimensionless form by

$$\ddot{x} + \delta\dot{x} + x = a\Omega^2 c_L, \tag{8}$$

$$\ddot{c}_L + (\alpha - \beta c_L^2 + \gamma c_L^4)\dot{c}_L + \Omega^2 c_L = b\dot{x}, \tag{9}$$

where δ is a damping parameter, a is a mass parameter, and $\Omega = \omega_s/\omega_0$ is the ratio of the Strouhal frequency to the natural frequency of the cylinder. The parameters α, β, γ, and b are constants which can be chosen to approximate a given problem.

The author believes that inclusion of the damping term $\gamma c_L^4 \dot{c}_L$ results in a wake oscillator model better able to capture the hysteresis effect. The hard excitation and soft excitation regimes seen in experimental results can be explained in terms of the three physically possible solutions of Eqs. (8) and (9): the zero solution and two additional positive solutions. The stability and instability of these solutions are investigated using the method of Liapounov. Hard excitation regimes of flow velocities (or frequency ratios f_s/f_0) are those where two stable states are possible for a given flow velocity (or frequency ratio): the position of rest and a vibration of finite amplitude. Soft excitation ranges are those where the rest position is unstable so that a finite oscillation is always generated. Sometimes the second state in the hard excitation ranges is not that of rest, but an oscillation with small amplitude at the same frequency as the high amplitude oscillation. This phenomena cannot be explained by the mathematical model.

Most recently, Facchinetti et al. [29] present an excellent review of the dynamics of wake oscillator models for 2D vortex-induced vibrations. More specifically, the authors examine three different types of coupling terms for the action f of the structure on the fluid wake oscillator. In general, the action term is the right-hand side of a given fluid–oscillator equation. For instance, $f = b\dot{x}$ for the Landl model as can easily deduced from Eq. (9). Velocity coupling $f = A\dot{x}$, displacement coupling $f = Ax$, and acceleration coupling $f = A\ddot{x}$ are considered. Velocity coupling is used extensively in the literature [52,56,57,54]. Displacement coupling has also been

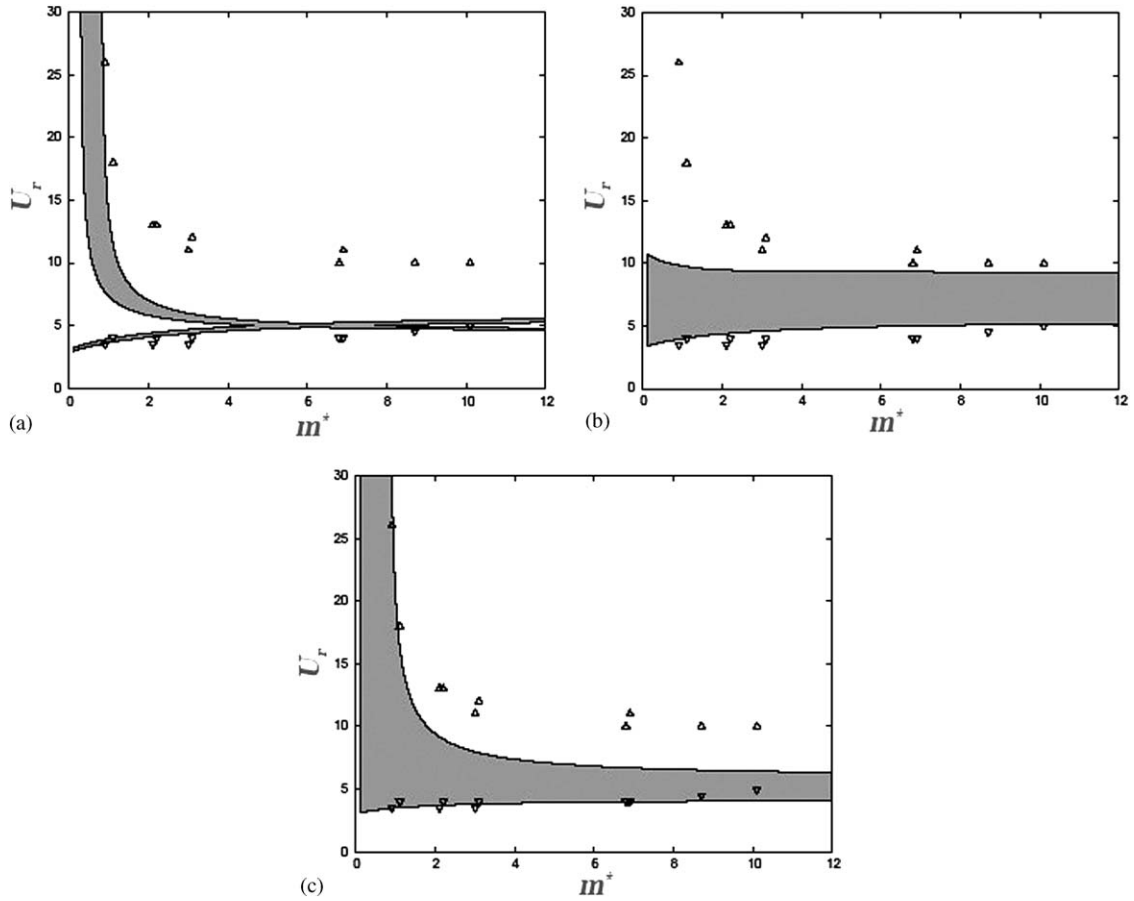

Fig. 9. Lock-in domains as a function of the reduced mass m^* for $S_G = 0.01$ and for the three different couplings: (a) displacement coupling, (b) velocity coupling, and (c) acceleration coupling. Comparison experimental data showing the upper and lower bounds of lock-in is represented by △ [29].

used [3]. With these different forms of coupling, the wake–oscillator models are compared with experimental data from the literature.

It is found that the displacement and velocity couplings fail to predict the lift phase seen in experimental results of vortex shedding from cylinders forced to oscillate. Displacement coupling fails to predict the lift magnification at lock-in and almost all prominent features of vortex-induced vibration at low values of the Skop–Griffin parameter S_G , while velocity coupling fails to predict the range of lock-in for low values of S_G. The Skop–Griffin parameter is a single combined mass-damping parameter often used in the literature and is given by $S_G = 8\pi^2 S^2 \mu\zeta$, where μ is the dimensionless mass ratio and $\zeta = r_s/2m\Omega_s$ is the structure reduced damping. r_s is the viscous dissipation in the supports, m is the mass of the structure plus the fluid added mass, and Ω_s is the structure natural angular frequency. Ω_s is defined as $\sqrt{h/m}$, where h is the total stiffness of the supports. The dimensionless mass ratio is defined by the authors as $\mu = (m_f + m_s)/\rho D^2$, where $m_f = C_M \rho \pi D^2/4$ is the fluid added mass, and m_s is the mass of the structure. $C_M = 1$ is the constant added mass coefficient from potential flow theory.

The key finding made by the authors is that the acceleration coupling succeeded in qualitatively modeling the features of VIV considered in the paper. Fig. 9 illustrates the difference between the lock-in domains predicted by the model equations for (a) displacement coupling, (b) velocity coupling, and (c) acceleration coupling for a representative low value of $S_G = 0.01$. Comparison experimental data showing the upper and lower bounds of lock-in are represented by the triangles. The reduced velocity is defined as $U_r = 2\pi U/\Omega_s D$.

3.1.2. Elastic cylinders

Several attempts have been made to extend the wake–oscillator models to elastic structural elements such as beams and cables. Iwan [58] extends the Iwan–Blevins model to predict the maximum VIV amplitude of taut strings and circular cylindrical beams with different end conditions. It is assumed that a strip theory approach can be applied to extend the equation of motion for the hidden flow variable z to the elastic structure. The strip theory approach assumes that there is no spanwise coupling in the flow, although the theory may fail to be accurate at small amplitudes of structural vibration since at these amplitudes the shedding process tends to be uncorrelated in spanwise composition. The structure is assumed to possess classical normal modes and the analysis is restricted to the cases in which the natural frequency of one of the modes is very near the shedding frequency, while all other modal frequencies are substantially removed from the shedding frequency. The author obtains an equation relating the maximum response amplitude for the structure in the nth mode, $Y_{n_{\max}}$, to various structural parameters:

$$\frac{Y_{n_{\max}}}{D} = \frac{a_4\sqrt{4/3}\gamma_n}{2\pi^3 S^2 \mu_r \zeta_n^T}\left[\frac{(a_1 - a_4)}{a_2} + \frac{a_4^2}{\pi^2 a_2 S \mu_r \zeta_n^T}\right]^{1/2}. \tag{10}$$

Interestingly enough, the details of the structure enter into Eq. (10) only through a dimensionless mode shape parameter γ_n, and the product of the mass ratio $\mu_r = 4m/\rho\pi D^2$ and the modal damping ratio of the structure ζ_n. ζ_n^T is taken to be the sum of ζ_n and damping due to interaction with the fluid. The a_i are dimensionless model parameters.

A comparison is made of a "universal" maximum response amplitude with various experimental results of maximum VIV for three structural elements: cables, pivoted rods, and rigid cylinders. The response amplitude curves $Y_{n_{\max}}/D/\gamma_n$ are plotted as a function of $\mu_r\zeta_n$ using Eq. (10) for each structural element (Fig. 10). Also shown in Fig. 10 is the empirical relationship $Y_{n_{\max}}/D/\gamma_n = 1/(1 + 1.60(\mu_r\zeta_n)^{1.80})$. The product $\mu_r\zeta_n$ is often referred to as the reduced damping and is almost identical to the Skop–Griffin parameter and the Scruton number discussed previously. The theoretical results show good agreement with experiments for amplitudes of response greater than 0.1 diameter. The data for the three different structural elements are shown to be consistent when normalized by the mode shape parameter.

Skop and Griffin [59] start with their version of a wake–oscillator model and proceed to extend it to elastic cylinders in an almost identical fashion. They obtain the following equation for the maximum oscillation amplitude in the ith pure mode:

$$\frac{Y_{i,\mathrm{MAX}}(x)}{D} = \frac{A_{\mathrm{MAX}}(S_{G,i})|\psi_i(x)|}{\sqrt{I_{iiii}}},$$

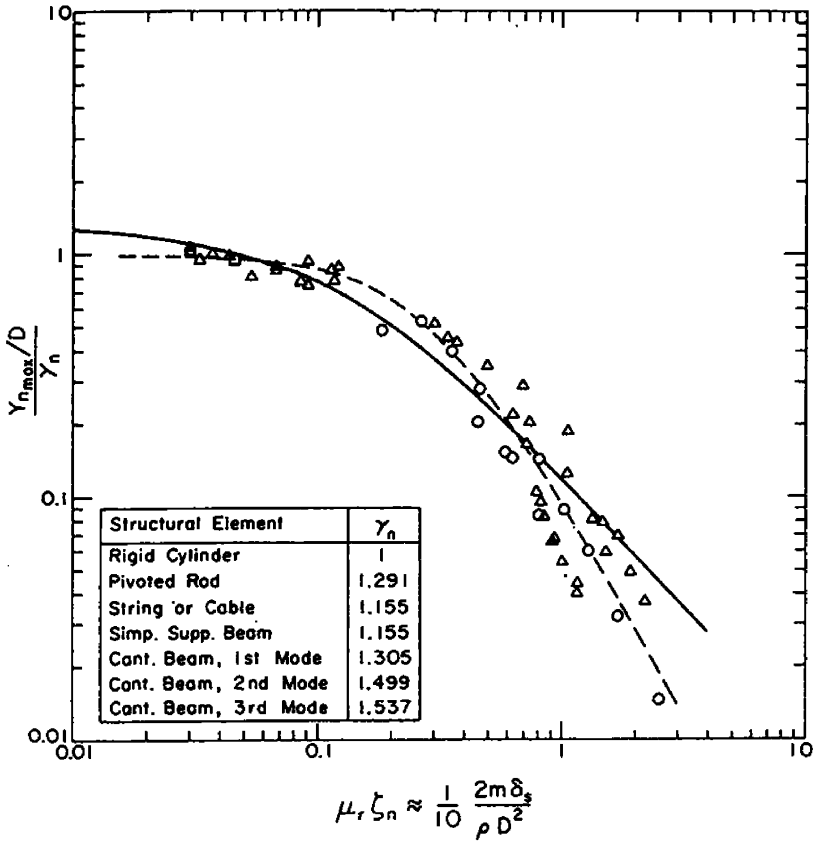

Fig. 10. Normalized maximum amplitude of response $Y_{n_{\max}}/D/\gamma_n$ vs. mass-damping parameter $\mu_r\zeta_n$ for different structural elements. ○, rigid cylinder experiments; △, pivoted rod experiments; □, cable experiments; —, theory; – –, empirical formula. $\gamma_n = 1$ (rigid cylinder), $\gamma_n = 1.291$ (pivoted rod) and $\gamma_n = 1.155$ (string or cable) [58].

where $\psi_i(x)$ is expression for the normalized mode. For example, $\psi_1(x) = x/L$ with $\psi_{i\neq 1} = 0$ for a pivoted rigid rod, and $\psi_i(x) = \sin(i\pi x/L)$ for a pinned–pinned beam. A_{MAX} is an amplitude parameter that is a function of the modal response parameter $S_{G,i} = \zeta_i/\mu_{ii}$. μ_{ii} is given by

$$\mu_{ii} = \frac{\bar{\rho}\bar{D}}{8\pi S^2 M_i} \int_0^L \rho^*(x)[D^*(x)]^3[\omega_S^*(x)]^2[\psi_i(x)]^2 \,\mathrm{d}x, \tag{11}$$

where $(\cdot)^*$ denotes a dimensionless variable, $\omega_S^*(x)$ is the shedding frequency, $\bar{\rho}$ is the average fluid density over the shedding region, $\bar{D}$ is the average cylinder diameter over the shedding region, and M_i is the effective mass in the ith mode. The integral in Eq. (11) is taken only over cylinder sections in which shedding occurs. I_{iiii} is defined by

$$I_{iiii} = \int_0^L [\psi_i(x)]^4 \,\mathrm{d}x \Big/ \int_0^L [\psi_i(x)]^2 \,\mathrm{d}x.$$

For example, $I_{iiii}^{-1/2} = I_{1111}^{-1/2} = 1.2910$ for a pivoted rigid rod. In general, good agreement is obtained with experimental data for flexible structures and cables, especially for $S_G < 0.5$ and $S_G > 2$.

Iwan [60] derives an analytical model for the VIV of non-uniform structures. In particular, he considers elastic systems that could be described by the 1D damped wave equation (e.g., cables). His model also allows for non-uniform flow profiles and accounts for inactive elements. Iwan finds that, for a particular pure response mode, the equations describing the system response reduced to those obtained for a rigid cylinder. In particular, for the nth mode,

$$\frac{\mathrm{d}^2\bar{y}_n}{\mathrm{d}t^2} + 2\zeta_n^T\omega_n\frac{\mathrm{d}\bar{y}_n}{\mathrm{d}t} + \omega_n^2\bar{y}_n = \left(\frac{\alpha_4}{v_n}\right)\frac{\mathrm{d}\bar{z}_n}{\mathrm{d}t}, \tag{12}$$

where α_4 is a model parameter, ζ_n^T is an effective (including fluid damping) structural damping, $\bar{y}_n(t)$ is the modal coefficient of the transverse displacement of the elastic system, $y(x,t)$, and $z_n(t)$ is the modal coefficient of the flow variable $z(x,y)$. v_n is a parameter representing the effective system mass and is defined as

$$v_n = \int_0^L m(x)\xi_n^2(x)\,\mathrm{d}x \Big/ \int_0^L s(x)\xi_n^2(x)\,\mathrm{d}x,$$

where $m(x)$ is the mass per unit length of the cable including the added fluid mass and any point masses, $s(x)$ is a function specifying which portions of the cable are being excited by locked-in vortex shedding, and $\xi_n(x)$ are the mode shapes. Eq. (12) is essentially the same equation that governs the response of an elastically mounted rigid cylinder, with the presence of the parameter v_n and the definition of ζ_n^T being the only differences.

The numerical results for various cable systems show that the response amplitude is strongly affected by cable non-uniformity. The reduction of the active region, the region over which vortex shedding occurs, and/or the addition of masses, generally reduces the amplitude of VIV.

Later models have added further refinements to the older models just described. Dowell [49] presents a method of constructing a fluid oscillator equation for C_L, which takes into account known theoretical and experimental behaviors of the fluid. Various self-consistency checks are performed on the model and numerical results are compared with those obtained from the Skop–Griffin model [54]. Several fundamental differences between the results are noted. Dowell's fluid oscillator is given by

$$\begin{aligned}\ddot{C}_L - \varepsilon[1 - 4C_L/C_{L_0}^2]\omega_s\dot{C}_L + \omega_s^2 C_L \\ = -B_1(D/V^2)y + \omega_s^2[A_1(\dot{y}/V) - A_3(\dot{y}/V)^3 + A_5(\dot{y}/V)^5 + A_7(\dot{y}/V)^7],\end{aligned} \tag{13}$$

where ω_s is the fluid frequency given by the Strouhal relationship, ε is a parameter to be determined, $\{A_1, A_3, A_5, A_7, B_1\}$ are slowly varying functions of Reynolds number and are held fixed, and C_{L_0} is the peak magnitude of the limit cycle oscillation obtained from Eq. (13) with $y = 0$ (a fixed cylinder). C_{L_0} is assumed to be a weak function of the Reynolds number and is assigned typical values.

Skop and Balasubramanian [61] present a modified form of the Skop–Griffin model [59] for flexible cylinders. The goal of the model is to accurately capture the asymptotic, self-limiting

structural response near zero structural damping. The fluctuating lift force C_L is separated into two components: one component satisfying a van der Pol equation driven by the transverse motion of the cylinder, and the other component which is linearly proportional to the transverse velocity of the cylinder (the stall term). Mathematically,

$$C_L(x,t) = Q(x,t) - \frac{2\alpha}{\omega_s}\,\dot{Y}(x,t),$$

where α is the stall parameter, ω_s is the intrinsic vortex-shedding frequency determined from the Strouhal relationship, $Q(x,t)$ is the component of C_L satisfying a van der Pol type equation, $\dot{Y}$ is the time derivative of the amplitude of structural motion, and x is the length variable along the structure.

Krenk and Nielsen [3] propose a double oscillator model in which the mutual forcing terms are developed based on the premise that energy flows directly between the fluid and structure. This means that the forcing terms correspond to the same flow of energy at all times. In dimensional form, the coupled equations are given by

$$m_0(\ddot{x} + 2\zeta_0\omega_0\dot{x} + \omega_0^2 x) = \tfrac{1}{2}\rho U^2 DL\,\frac{\dot{w}}{U}\,\gamma, \tag{14}$$

$$m_f\left[\ddot{w} - 2\zeta_f\omega_s\left(1 - \frac{w^2 + \dot{w}^2/\omega_s^2}{w_0^2}\right)\dot{w} + \omega_s^2 w\right] = -\tfrac{1}{2}\rho U^2 DL\,\frac{\dot{x}}{U}\,\gamma, \tag{15}$$

where x is the structural displacement, w is the transverse motion of a representative fluid mass m_f, ζ_f is the fluid damping ratio, ω_s is the undamped angular frequency of the fluid oscillator (determined from the Strouhal relation), γ is a dimensionless coupling parameter taken as a constant, and the parameters m_0, ζ_0, and ω_0 have their usual meanings. The parameter w_0 controls the amplitude of the self-induced vibrations of the fluid oscillator in the case of a stationary cylinder. Note that a quadratic fluid damping term has been included in the formulation. Energy generation over a period begins with the negative damping (provides the self-excitation) term in Eq. (14). This energy is extracted by means of the right-hand side (RHS) of Eq. (14). The transfer of energy to the cylinder occurs via the RHS of Eq. (15). This energy is then dissipated by the structural damping term.

Values for the model parameters are taken from experiments, and the model results display branching from below and above the lock-in region. The solution in the lock-in region is unstable, which the authors claim will lead to transition between the two modes of oscillation. However, changes in model parameters do not show effects similar to changes in experimental parameters.

3.2. Sdof models

Proponents of this type of modeling include Scanlan and Simiu [62], Basu and Vickery [63], and Goswami et al. [64]. Sdof models use a single ordinary differential equation to describe the behavior of the structural oscillator.

Using the notation of Goswami et al. [64], the general form of such models is given by

$$m(\ddot{x} + 2\zeta\omega_n\dot{x} + \omega_n^2 x) = F(x,\dot{x},\ddot{x},\omega_s t), \tag{16}$$

where m is the mass of cylinder, x is the transverse (lift direction) displacement, ω_s is the Strouhal frequency, and F is an aeroelastic forcing function. The influence of the wake dynamics is incorporated into Eq. (16) via the appropriate choice of the function F. They propose a model for the VIV of a flexibly supported cylinder that is a hybrid of the nonlinear sdof model of Scanlan and Simiu [62] and the coupled wake oscillator model of Billah [25]. The general form of this model is given by

$$m(\ddot{x} + 2\zeta\omega_n\dot{x} + \omega_n^2 x) = \tfrac{1}{2}\rho U^2 D\left[Y_1(K)\frac{\dot{x}}{D} + Y_2(K)\frac{x^2}{D^2}\frac{\dot{x}}{U} + J_1(K)\frac{x}{D} + J_2(K)\frac{x}{D}\cos(2\omega_s t)\right]. \tag{17}$$

In Eq. (17), $K = \omega_n D/U$ is the reduced frequency, $Y_1(K)$ is a linear aeroelastic damping term, $Y_2(K)$ is a nonlinear aeroelastic damping term, $J_1(K)$ is an aeroelastic stiffness term, and $J_2(K)$ is a parametric stiffness term. In essence, $Y_1(K)$ and $Y_2(K)$ represent the self-excitation and self-limitation characteristics of the response. $J_2(K)$ represents the coupling between the wake and the cylinder, and represents the key contribution of the wake oscillator. $J_1(K)$ represents the shift in the mechanical response frequency from the zero-wind frequency f_n. In other words, $J_1(K)$ represents any shift in the cylinder natural frequency from its zero-wind (resting state) value. The parameter values (Y_1, Y_2, J_1, J_2) are estimated through a range of reduced velocities and damping from experimental results [65] and the method of slowly varying parameters.

The results indicate a negligible frequency shift and consequently J_1 can be taken as zero. The remaining parameters (Y_1, Y_2, J_2) are collectively found to influence the peak amplitude of the response at lock-in, the location of the maximum response, and the band of appreciable response. The authors do not compare the performance of their model with experimental results from the literature.

Bearman [5] considers the following equation for a flexibly mounted bluff body (not necessarily a circular cylinder):

$$M\ddot{y} + 4\pi N_0\delta_s M\dot{y} + 4\pi^2 N_0^2 My = C_y\rho U^2 D/2, \tag{18}$$

where y is the displacement in the transverse direction, N_0 is the undamped natural frequency of the body, M is the mass per unit length of the body, δ_s is the fraction of critical damping, and C_y is the transverse force coefficient for the bluff body due to the shedding vortices. Assuming that for large enough amplitudes the fluid force and the body displacement both oscillate at a certain frequency n_v, and that the fluid force must lead the cylinder motion by some phase angle ϕ, solutions of the form $y = \bar{y}\sin(2\pi n_v t)$ and $C_y = \bar{C}_y\sin(2\pi n_v t + \phi)$ are sought. The following relationships are obtained by replacing the assumed solutions into Eq. (18):

$$\frac{N_0}{n_v} = \left[1 - \frac{\bar{C}_y}{4\pi^2}\cos(\phi)\left(\frac{\rho D^2}{2M}\right)\left(\frac{U}{N_0 D}\right)^2\left(\frac{y}{D}\right)^{-1}\right]^{-1/2}, \tag{19}$$

$$\frac{\bar{y}}{D} = \frac{\bar{C}_y}{4\pi^2}\sin(\phi)\left(\frac{\rho D^2}{2M\delta_s}\right)\left(\frac{U}{N_0 D}\right)^2\frac{N_0}{n_v}, \tag{20}$$

where $\rho D^2/2M$ is the mass ratio, $\rho D^2/2M\delta_s$ is the mass-damping parameter, and $U/N_0 D$ is the reduced velocity. Clearly, the frequency ratio N_0/n_v and the amplitude ratio $\bar{y}/D$ depend on the

mass ratio. As seen from Eq. (19), a large value of the mass ratio means that the frequency of oscillation of the cylinder is appreciably different from its natural frequency. It is only for small values of the mass ratio that $N_0 \approx N_v$. Eq. (20) shows that it is that part of the fluctuating transverse force coefficient that is in-phase with the cylinder velocity which affects the amplitude ratio.

Chen et al. [66] present an unsteady flow theory for the structural response of a 1 dof circular cylinder to vortex shedding. The model correctly pointed out the fluid-elastic instabilities in the lock-in region. For low oscillation amplitudes, as the flow passes through the lock-in region, the modal damping may become negative and the system is unstable. The amplitude continues to grow until it becomes large enough so that modal damping values increase and the system is stabilized.

3.2.1. *Specific applications of sdof models*

Cai and Chen [67] study the wind-induced large-amplitude response of a stack supported by cable guy wires at four levels. An unsteady flow theory developed in Chen et al. [66] is used to model the VIV of the stack. The theory is essentially an sdof model in which the effects of the flowing fluid are characterized as the fluid damping and stiffness, and these parameters are in turn dependent on oscillation amplitude, reduced flow velocity, and Reynolds number. For the stack considered by itself, it is found that the third mode, with natural frequency ≈ 2.2 Hz, is most vulnerable to vortex-shedding-induced resonance due to a large modal participation factor. The stack vibration can then be said to be due primarily to vortex shedding at the lower portion, which is mostly associated with the third mode. For the stack–cable system, both the stack and the cables show characteristic peaks in their spectra at the lock-in resonances of the stack modes. Parametric resonances (secondary peaks) in the cables are a result of stack motion at the ends of the cable supports. In general, primary parametric resonances occur in the cables, whose natural frequencies are approximately half the lock-in frequency (i.e., the shedding frequency) of a given stack mode. Wind speed, cable tension, and damping are found to affect the parametric resonances. The parametric resonances in the cables may be significantly reduced by changing their natural frequencies through careful adjustment of the tensions.

A technique for the extraction of aeroelastic parameters from wind tunnel tests is described in Gupta et al. [68]. These parameters are used in the sdof mathematical model for the VIV of a structure at lock-in. The authors use Scanlan's model,

$$m(\ddot{z} + 2\zeta\omega_n\dot{z} + \omega_n^2 z) = \tfrac{1}{2}\rho U^2 D\left[Y_1\left(1 - \varepsilon\frac{z^2}{D^2}\right)\frac{\dot{z}}{U} + Y_2\frac{z}{D}\right] = F(z, \dot{z}, U, t). \tag{21}$$

The instantaneous fluctuating lift force term, $\frac{1}{2}C_L\sin(\omega t + \phi)$, has been neglected in this formulation since it is generally smaller than the aerodynamic lift caused by the motion of the body (i.e., $F(z, \dot{z}, U, t)$). The unknown parameters in Eq. (21) are the linear aeroelastic damping, Y_1, and the nonlinear aeroelastic damping, ε. The linear aeroelastic stiffness, Y_2, can be easily determined from oscillation frequency measurements. The technique described in the paper is based on the concepts of invariant imbedding and nonlinear filtering theory and is shown to be effective even for turbulent (noisy) conditions. Furthermore, the method works regardless of the initial conditions of the experiments (decaying method vs. self-excited method) and in situations where the steady-state amplitude is very small. The calculated values of the parameters Y_1 and ε

are presented as a function of the Scruton number, $S_c = 4\pi m\zeta/\rho D^2$, for a variety of section models, including laminar flow over a smooth cylinder and turbulent flow over a smooth cylinder.

3.3. Force–decomposition models

Sarpkaya [27] is credited with introducing the force–decomposition model. In his model, the lift force on an elastically mounted rigid cylinder is decomposed into a fluid inertia force related to the cylinder displacement and a fluid damping force related to the cylinder velocity. The lift coefficient, C_L, is expressed as

$$C_L = C_{ml}\pi^2 \frac{U_m T}{D}\left(\frac{D}{\bar{V}T}\right)^2 \sin\{\omega t\} - \frac{8}{3\pi} C_{dl}\left(\frac{U_m T}{D}\right)^2\left(\frac{D}{\bar{V}T}\right)^2 \cos\{\omega t\}, \tag{22}$$

where C_{ml} is the inertia coefficient, C_{dl} is the drag coefficient, T is the period of the transverse motion of the cylinder, $U_m = 2\pi A/D$, and $V_r = \bar{V}T/D$ is the reduced velocity. A is the maximum amplitude of the cylinder motion, and $\bar{V}$ is the velocity of the ambient flow. Eq. (22) can then be incorporated into the equation of motion for an elastically mounted, linearly damped, and periodically forced cylinder, yielding

$$\ddot{x}_r + 2\zeta\dot{x}_r + x = \rho_r\Omega^2\left(C_{ml}\sin\{\Omega\tau\} - \frac{16}{3\pi^2} X_r C_{dl}\cos\{\Omega\tau\}\right). \tag{23}$$

In Eq. (23), $x_r = x/D$, Ω is the ratio of the cylinder oscillation frequency to its natural frequency f_c/f_n, ρ_r is the ratio of the fluid density to the density of the cylinder ρ_f/ρ_c, and $\tau = \omega_n t$. If the values of C_{ml} and C_{dl} corresponding to the V_r value at perfect synchronization can be determined from experiments, then Eq. (23) can be solved, and the response of the cylinder in the synchronization region ascertained.

Sarpkaya shows through a parametric study that the maximum response of the cylinder is governed by a single parameter, the stability (mass-damping) parameter S_G, for values of this parameter larger than about unity. This stability parameter is defined as $S_G = \zeta/a_0$, the ratio of the material damping and a mass ratio. For low values of the stability parameter, the mass ratio a_0 and damping ζ affect the response separately. It is important to note that S_G, as defined by the author, can also be written as $S_G = 8\pi^2\zeta S^2 M/\rho D$. In this form, it can be recognized as the Skop–Griffin parameter.

Griffin and Koopman [69] and Griffin [70] split the fluid force into an excitation part and a reaction part that includes all the motion-dependent force components. In non-dimensional form, the equation of motion for an elastically mounted rigid cylinder is written as

$$\ddot{y} + 2\omega_n\zeta_s\dot{y} + \omega_n^2 y = \mu\omega_s^2(C_L - C_R),$$

where C_L is the lift coefficient, C_R is the reaction coefficient, ω_s is the Strouhal frequency, ζ_s is the structural viscous damping, and μ is a mass parameter equal to the inverse Skop–Griffin parameter (i.e., $\mu = 1/S_G$). The fluid dynamic reaction (damping) force in phase opposition with the cylinder velocity is measured as a function of incident flow speeds (Re: 300–1000), including the lock-in speed. Also measured is the lift component in phase with the cylinder velocity. This is the component of the lift coefficient that is associated with energy transfer to the vibrating cylinder.

Wang et al. [71] introduce a nonlinear fluid force model for the VIV of a single elastically supported rigid cylinder in a uniform crossflow. The vibration of the cylinder in the transverse (y) and streamwise (x) directions is analyzed using a 2 dof structural model. The equations of motion are obtained from Euler–Bernoulli beam theory and the effects of vibration mode are accounted for through a modal analysis approach. The uncoupled equations of motion are given in dimensionless form by

$$\ddot{X}_n(z,t) + 2\zeta_{sn}\omega_{n0}\dot{X}_n(z,t) + \omega_{n0}^2 X_n(z,t) = f_{xn}(z,t)/2M_r,$$

$$\ddot{Y}_n(z,t) + 2\zeta_{sn}\omega_{n0}\dot{Y}_n(z,t) + \omega_{n0}^2 Y_n(t) = f_{yn}(z,t)/2M_r,$$

where z is along the axis of the cylinder, ζ_{sn} is the structural damping in the nth mode, M_r is structural mass ratio, ω_{n0} is the natural frequency of a stationary cylinder, $f_{xn}(z,t)$ is the fluid-force coefficient in the streamwise direction in the nth mode, and $f_{yn}(z,t)$ is the fluid-force coefficient in the transverse direction in the nth mode. Note that for an elastically mounted rigid cylinder ($n=1$), $f_{x1}(t) = c_D(t) - c_L(t)\dot{Y}_1(t)$ and $f_{y1}(t) = c_D(t)\dot{Y}_1(t) - c_L(t)$, where $c_D(t)$ is the drag force coefficient and $c_L(t)$ is the lift force coefficient. It is also worth mentioning that, for a stationary rigid cylinder, the transverse and streamwise fluid force coefficients will coincide with the lift and drag force coefficients, respectively.

A 2 dof model is used because it has been found that streamwise oscillations have a substantial effect on the transverse vibrations and their characteristics [72]. Higher harmonics representing the nonlinearity in the fluid–structure interaction are accounted for in the form of nonlinear expressions for the fluid-forcing terms. The fluid-force components of the model are obtained from amplitude and frequency data for a freely vibrating cylinder in crossflow by carrying out a spectral analysis of the time series of structural vibrations using the auto-regressive moving average (ARMA) technique. Analysis of the power spectral density of the cylinder response indicates the presence of higher harmonics in both the resonance and off-resonance responses. Specifically, the vortex-shedding frequency and higher harmonics of the shedding frequency are present in the resonance response. The off-resonance response shows the presence of the vortex-shedding frequency and higher normal modes of the structure. The fluid-force components of the model are found to be dependent on structural damping and mass ratio. The model is used to predict the VIV of an elastic cylinder which is fixed at both ends and the results were compared with experimental results and the sdof model of Sarpkaya. The experimental results of Goswami et al. [65] verify the presence of both the shedding frequency and the natural frequency of the structure in the spectrum of the cylinder vibration within lock-in and outside lock-in. The structural response thus contains two distinct frequencies and these are manifested in the form of a beat. This is verified by the Benaroya–Wei [73] model discussed next.

3.4. Variational approach

A semi-analytical approach for modeling vortex-induced vibration has been derived by Benaroya and Wei [73]. This approach is based on the extension of Hamilton's principle to systems of changing mass and, unlike the models discussed previously, makes no a priori assumptions about the form of the governing equations. The extended form of Hamilton's principle for such systems is first derived by McIver [74]. The principle of virtual work for an open

control volume $R_o(t)$ having a portion of its boundary which is closed to mass transfer, $B_c(t)$, and a portion which is open to mass transfer, $B_o(t)$, is

$$\delta(L)_0 + \delta W_{nc} + \iint_{B_o(t)} (\rho \mathbf{U}) \cdot \delta \mathbf{r}(\mathbf{U} - \mathbf{V}) \cdot \mathbf{n} \, \mathrm{d}s - \frac{\mathrm{d}}{\mathrm{d}t} \iiint_{R_o(t)} (\rho \mathbf{U}) \cdot \delta \mathbf{r} \, \mathrm{d}v = 0. \tag{24}$$

δW_{nc} is the virtual work done by non-conservative forces and $(L)_0$ is the Lagrangian of the system contained within the open control volume. The only virtual work contributions are those from surface tractions on the open and closed portions of the control volume boundary. By letting the virtual displacements coincide with the actual displacements (i.e., $\delta \mathbf{r} = \mathbf{U} \, \mathrm{d}t$), an energy equation can be recovered from the virtual work equation.

Consider next the steady viscous flow around a rigid cylinder. The control volume is chosen to include part of the fluid arbitrarily far from the cylinder and the cylinder itself. The cylinder is considered to be a closed control surface and if the control volume is large enough to include other solid boundaries, these will also be part of the closed control surface. The energy equation for this case becomes

$$\begin{aligned} &\frac{\mathrm{d}}{\mathrm{d}t}(T_{\text{cylinder}} + V_{\text{cylinder}})_o + m_{\text{fluid}} U \dot{U} \\ &\quad = \iint_{B_c(t)} (-p\mathbf{n} + \boldsymbol{\tau}) \cdot \mathbf{U} \, \mathrm{d}s + \iint_{B_o(t)} (-p\mathbf{n} + \boldsymbol{\tau}) \cdot \mathbf{U} \, \mathrm{d}s \\ &\qquad + \iint_{B_o(t)} \rho\left(\tfrac{1}{2} U^2\right)(\mathbf{U} - \mathbf{V}) \cdot \mathbf{n} \, \mathrm{d}s, \end{aligned} \tag{25}$$

where the potential energy of the fluid in the open control volume has been assumed constant, and the potential energy per unit mass of the fluid e over the open control surface has been neglected. $-p\mathbf{n}$ is the inward normal pressure and $\boldsymbol{\tau}$ is the shear force vector on the control surfaces. Once expressions for the kinetic and potential energies of the cylinder have been substituted into Eq. (25), the equation of motion for the cylinder is obtained. The expressions on the right-hand side of the equation of motion are obtained experimentally. Further details are given in the experimental section of this review (Section 2) and in Refs. [48,75]. Once these terms are obtained, the equation of motion is integrated twice numerically in time to obtain displacement.

Fig. 11 is a comparison of the response predicted by the reduced-order model and those obtained from phase-averaged cylinder position vs. time measurements. The model problem used consists of a low-mass-damping cylinder ($m^*\zeta = 0.0377$) mounted as an inverted pendulum.

Both the oscillation frequency and the oscillation amplitude are accurately predicted by the model along with the beating behavior. Singularities at the points of maximum displacement of the cylinder lead to numerical instabilities that are responsible for the clipping of the reduced-order response.

4. Numerical methods

Numerical methods are an alternative way to solve the fully coupled problem of VIV of bluff bodies. For flow-induced vibration, four basic issues should be considered in any numerical

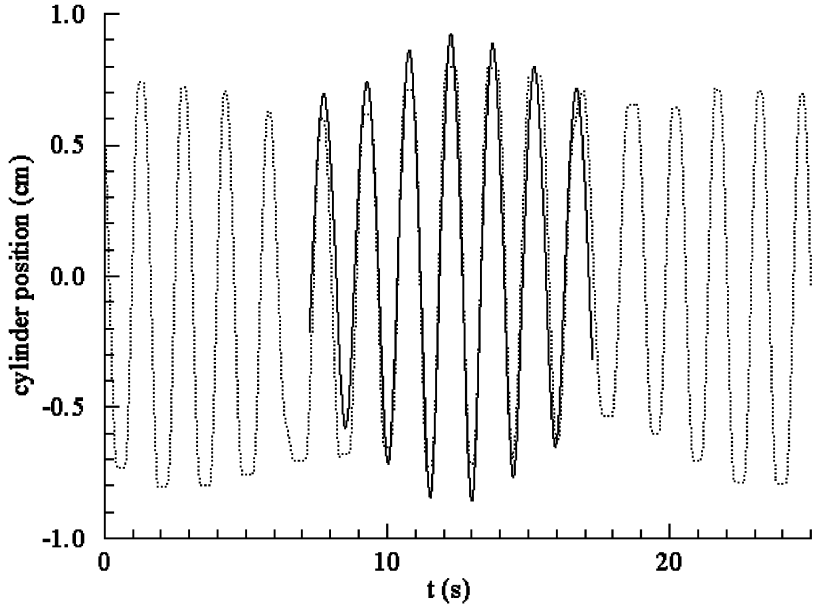

Fig. 11. Comparison of the reduced-order model response (dotted line) and the phase-averaged cylinder position vs. time measurements (solid line) [48].

simulation: modelling of the flow field, modelling of the structural vibration, modelling of the fluid–structure interaction, and data analysis [76].

The flow field behind a stationary cylinder and the flow field behind a cylinder forcibly oscillated at a specified amplitude and frequency (the forced vibration problem) have received considerable attention from computationalists. However, the natural approach to a prediction of VIV in self-excited vibration is a method that couples the fluid motion and the motion of the cylinder. This coupled approach has been taken by most of the recent investigations into the VIV problem [77]. Among the major methods used are time-marching schemes (see, for example, Ref. [78]), direct numerical simulation (for example, Ref. [79]), and the vortex-in-cell method (VIC). Most of these numerical simulations are usually restricted to the lower end of the Reynolds number spectrum. However, large eddy simulation (LES) has been used to solve the forced vibration problem at high Reynolds numbers (Ref. [80] at $Re = 2.4 \times 10^4$) and the self-excited problem at moderate Reynolds numbers (Ref. [77] at $Re = 8000$). From a numerical point of view, limits arise in the flow-field simulation of 3D domains with large aspect ratios [29].

4.1. The VIC method

The VIC method is a numerical method in which the flow field is described by a cloud of moving vortex elements.The detailed numerical formulation of the VIC method is quite complex and beyond the scope of this review. Details can be found in Meneghini and Bearman [81] and Sarpkaya [82,83]. Zhou et al. [72] use the VIC method to solve the problem of 2D incompressible flow past an elastic circular cylinder. The structure is modeled as a spring–damper–mass system

with two translational degrees of freedom. A constant Reynolds number of 200 is chosen for all simulations, based on the fact that at this Reynolds number the shedding vortices are still two-dimensional and the wake is laminar. A finite-difference scheme is implemented to solve the vorticity transport equation. The forcing terms on the right-hand side of the cylinder equations of motion at each time step are obtained from the flow field calculations through the integration of the pressure and wall shear stress around the cylinder surface. The reference frame is fixed with the cylinder and, consequently, after the cylinder motion is determined at each time step, a flow equal and opposite to the cylinder motion must be superimposed to the flow field. The frequency characteristics of the force, displacement and velocity fields are obtained using the ARMA technique mentioned previously. The fluid motion is then solved in the next time step accounting for these effects. The process is repeated in an iterative way.

The results of the numerical simulations indicate that the cylinder response is strongly dependent not only on the Skop–Griffin parameter (reduced damping), but also on the mass ratio. It is the natural frequency of the fluid–structure system f_n^* and not the structural natural frequency f_n that is very close to the natural shedding frequency f_s^* when the peak structural response occurs. The importance of the fluid damping, through the Skop–Griffin parameter, is illustrated by noting that even when the natural frequency of the fluid–structure system is near the natural shedding frequency, a limit-cycle oscillation (i.e., a self-limited oscillation) results. The amplitude of the limit-cycle oscillation decreases as the Skop–Griffin parameter increases. In general, the 1 dof (transverse motion only) model is only able to qualitatively reproduce some of the results obtained with the 2 dof model. This suggests that the streamwise motion does indeed influence the motion in the transverse direction.

4.2. Direct numerical simulation

Evangelinos et al. [84] use direct numerical simulation (DNS) based on spectral elements to simulate the 3D flow past rigid and flexible cylinders. The simulations are conducted at a Reynolds number of 1000, where the flow exhibits a turbulent wake, and the cylinder is allowed only vertical motions in the crossflow direction. The main assumptions are that there is no structural damping and that the structural eigenfrequency is "locked-in" to the Strouhal number of the corresponding stationary cylinder flow. Simulations are conducted for a rigid cylinder of normalized spanwise length $L_z = 4\pi$, where the cylinder diameter d is used as the scaling factor. Simulations for flexible cylinders are conducted for the following cases: (1) a short cylinder of spanwise length $L_z = 4\pi$ with free ends, (2) a long cylinder of spanwise length $L_z = 378$ with free ends, (3) a short cylinder of spanwise length $L_z = 4\pi$ with pinned ends, and (4) a long cylinder of spanwise length $L_z = 378$ with pinned ends.

Table 1 presents a summary of the results of the simulations. It is stated that the errors in the given values are less than 10%. Note that the rms lift coefficient $(C_l)_{\text{rms}}$ for the freely oscillating rigid cylinder is much larger than it is for the other cases, while the stationary cylinder has the smallest value. The same can be said for the mean and rms values of the drag coefficients, C_d and $(C_d)_{\text{rms}}$, respectively.

Guilmineau and Quetey [85] consider the vortex shedding from the forced oscillation of a circular cylinder in two distinct cases: the flow induced by the harmonic in-line oscillation of a cylinder in a quiescent body of water, and the flow induced by a transversely oscillating cylinder in

Table 1
Summary of time- and span-averaged amplitude, lift and drag coefficients at lock-in [84]

Cylinder type	y_{max}/d	y_{rms}/d	$(C_l)_{rms}$	C_d	$(C_d)_{rms}$
Stationary	0	0	0.12	1.04	0.02
Rigid	0.75	0.51	1.53	2.11	0.65
Short beam—free	0.93	0.51	0.83	1.86	0.48
Short beam—fixed	1.09	0.43	0.86	1.81	0.43
Long beam—free	0.61	0.36	0.93	1.75	0.51
Long beam—fixed	0.85	0.25	1.16	1.62	0.44

a uniform flow of Reynolds number 185. In both cases, the 2D unsteady Navier–Stokes equations are solved using a control volume approach with an algorithm (consistent physical interpolation (CPI)) implemented to reconstruct the velocity fluxes. For the in-line oscillation study, the Reynolds number is fixed at 100 and the Keulegan–Carpenter (KC) number is fixed at 5. The Reynolds number is defined by $Re = U_m D/v$ and the Keulegan–Carpenter number is defined by $KC = U_m/f_e D$, where U_m is the maximum oscillatory velocity, v is the kinematic viscosity, and f_e is the frequency of the oscillatory flow.

At the KC number used in the study, a periodic vortex formation is observed, consisting of vortices with symmetrical locations with respect to the line of motion of the cylinder. The in-line force time history acting is computed and the results compared with that predicted by the Morison equation. Agreement is generally good, except for the extremes of the time history. For the transverse oscillation study, the mechanisms of vortex switching are examined as a function of the ratio of the vortex shedding or excitation frequency (f_e) to the natural shedding frequency from a stationary cylinder (f_0), f_e/f_0. As f_e/f_0 increased, the concentration of vorticity in the wake of the cylinder moves closer to the cylinder, resulting in a tighter vortex structure (Fig. 12). A limiting position is reached and the vorticity concentration abruptly switches to the opposite side of the cylinder.

Willden and Graham [86] use a quasi-3D extension of the strip theory to simulate the low Reynolds number VIV of a long flexible circular cylinder with a low mass ratio and zero damping. In strip theory, the cylinder is divided into segments along its length and each strip is treated as an individual cylinder for flow calculations and then the complete cylinder is reconstructed by reassembling the segments [77]. The reduced velocity is defined as $V_r = U/f_n D$, where f_n is the natural frequency of the cylinder in air. The mass ratio is defined as $m^* = 2m/\rho D^2$, where m is the mass per unit length of the cylinder. The 2D simulations for the free transverse vibration of the flexibly mounted cylinder indicate that, for very low mass ratios ($m^* = 1$ in this case), the fluid (through the added mass) is dominant over the structure in controlling the oscillatory frequency throughout lock-in. In other words, the oscillatory and vortex-shedding frequencies remain locked-in to one another throughout the reduced velocity range simulated, $V_r = 2.5$–16. This phenomenon does not occur in systems with high mass ratios. For such systems, the vortex-shedding frequency is entrained by the structural frequency, $f_v \approx f_n$. It is also seen that the body oscillates at approximately the natural frequency of the combined fluid and structure system throughout lock-in. In other words, $f_v \approx f_N$ throughout lock-in, where $f_N = \sqrt{f_n^2/(1 + m_a/m)}$ is

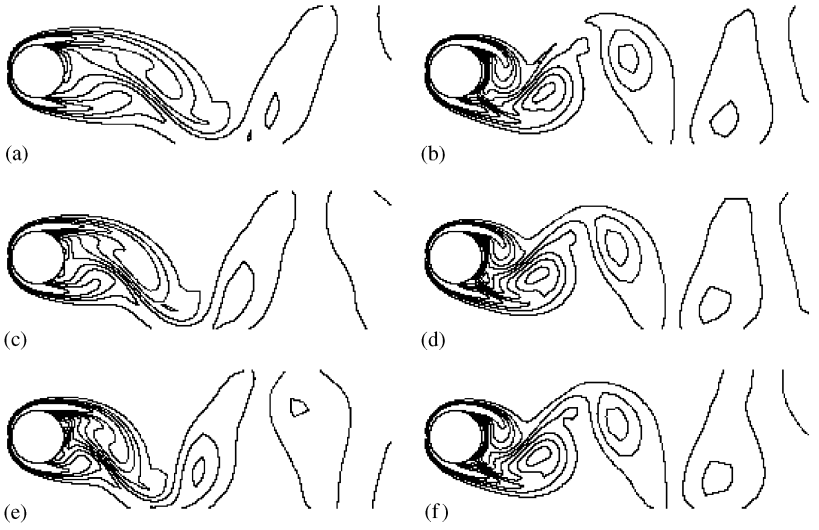

Fig. 12. Instantaneous vorticity contours for $Re = 185$ and $A_e/D = 0.2$. In all frames, the location of the cylinder is at its extreme upper position. Values of f_e/f_0 equal to: (a) 0.80, (b) 0.90, (c) 1.00, (d) 1.10, (e) 1.12, (f) 1.20 [85].

the effective natural frequency and m_a is the added mass. By decomposing the component of lift coefficient in phase with the cylinder motion into contributions from pressure and shear forces, it is found that the shear force component in-phase with the cylinder velocity effectively acts as hydrodynamic damping, balancing the positive excitation force provided by the pressure force in phase with the cylinder velocity. These shear and pressure forces are found to be quite large in magnitude. Shear flow simulations past the 3D cylinder are also performed and cellular shedding in the wake is observed. Despite the presence of the shear flow, the vortex shedding remained correlated over a substantial length of the cylinder.

Blackburn et al. [87] present a complementary numerical and experimental study of the VIV of a rigid cylinder at low Reynolds number flow (~ 500). The fluid and mechanical (mass ratio, mass-damping) dynamic parameters are matched in both the simulations and the experiments. 2D flow simulations were unable to predict the nature of the multibranched plot of amplitude A^* vs. SV_r. The Strouhal number S for a fixed cylinder is used to normalize the reduced velocity V_r, thus leading to the product SV_r. The reasoning behind this normalization is that the 2D and 3D simulations actually have different Strouhal numbers for the same Reynolds numbers, 0.225 and 0.205, respectively. 3D flow simulations generate results similar to the experimental results, in spite of the fact that the cylinder end boundary conditions are not exactly the same as in the experiments and the axial resolution and extent of the simulations are less than desirable. The 3D simulations coincide with the experimental results in the prediction of a $2P$-type vortex-shedding mode for a representative SV_r value of 1.27 along the lower branch of the response curve. The $2P$-type vortex-shedding mode is first reported in Williamson and Roshko [38] and corresponds to two pairs of counter-rotating vortices per shedding cycle.

Blackburn and Henderson [88] conduct a detailed numerical study of the phase change of vortex shedding with respect to cylinder motion commonly observed in experimental studies of

flows past stationary and oscillating cylinders. By phase change, it is meant the change in the phase angle ϕ between the cylinder cross-flow displacement $y(t)$ and the fundamental harmonic of the lift force F_L. The Reynolds number is fixed at 500 and the oscillation amplitude of the cylinder is fixed at $y_{\max}/D = 0.25$. Experimental studies have indicated that the timing of vortex formation switches phase by approximately 180° over a narrow band of structural oscillation frequencies in the primary lock-in regime. In other words, there exists a certain frequency range such that, for a fixed point in the cylinder motion cycle, the side of the cylinder where the first vortex is formed will change abruptly. The switch is found to affect the sign of the mechanical energy transfer between the cylinder and the surrounding fluid, as well as the phase of the vortex-induced forces on the cylinder. Furthermore, the timing of this phase shift is strongly affected by the frequency ratio $F = f_0/f_v$, where f_0 is the cylinder cross-flow oscillation frequency and f_v is the natural shedding frequency from a fixed cylinder. The dimensionless form of the mechanical energy transferred from the flowing fluid to an oscillating cylinder per motion cycle is given as

$$E = \tfrac{1}{2} \oint (C_L \, \mathrm{d}\alpha + \alpha \, \mathrm{d}C_L), \tag{26}$$

where C_L is the lift coefficient and α is an instantaneous dimensionless displacement variable $\alpha(t) = y(t)/D$. Positive values of E correspond to work done on the cylinder, while negative values correspond to work done on the surrounding fluid. It can be shown that E is positive when ϕ is in the range 0–180°. The sign of E is ascertained from the phase plane plot of $y(t)$ vs. C_L, which is in the form of a limit cycle during frequency entrainment (lock-in). The sign of E is positive if the direction of traverse in the limit cycle is clockwise. By considering the range $0.75 < F < 1.05$ and calculating E for each increment (or decrement) ΔF from two initial points $F = 0.875$ and $F = 0.975$, a bifurcation solution with hysteresis effects is found in the transition to these states.

Four solution branches corresponding to periodic shedding states are observed: two branches associated with Kármán street wakes (K_1 and K_2), a branch characterized as the asymmetric two-cycle mode (A_1), and a branch characterized as the asymmetric synchronized branch (A_2). The K_1 branch has negative values of E at lower frequencies and progresses to positive values at higher frequencies. The A_1 and A_2 branches always have positive values of E. The K_2 branch always has negative values of E. The transitions between the branches is rather complicated and cannot be easily categorized. Of interest is a band of frequencies $0.905 < F < 0.95$, termed the weakly chaotic oscillator range, in which the sign of E changes between the K_1 and K_2 branches. In this band, the sign of E and the phase angle ϕ undergo transition from positive to negative values in a discontinuous fashion. Fig. 13 shows the different branches in the F–E plane. It is suggested that the relaxation oscillator behavior seen in this range is indicative of different mechanisms vying for control of the wake dynamics. The competing mechanisms are the relative magnitudes of the pressure-gradient and the surface-acceleration vorticity generation. Several tests are performed to test the validity of this hypothesis, and results presented do lend validity to this claim.

4.3. The finite element method

Barhoush et al. [89] use an approach based on the finite element method and Scanlan's vortex-shedding empirical model to analyze the VIV response of plane frame (2D) structures. The equations of motion for a plane frame element, having 2 dof per node, are obtained from

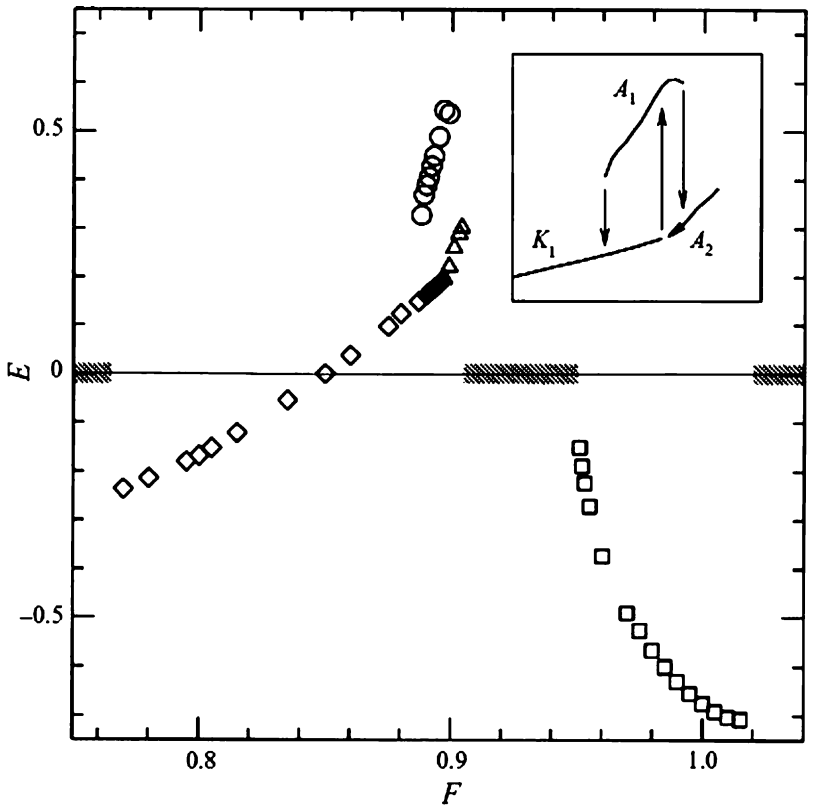

Fig. 13. Energy transfer coefficient E as a function of the frequency ratio F for periodic wake flows. ◇, Kármán street mode, branch K_1; □, Kármán street mode, branch K_2; ○, asymmetric two-cycle mode, branch A_1; △, asymmetric synchronized mode, branch A_2; frequency ratios for aperiodic regimes are shown hatched. Inset shows paths followed during sweeps of the frequency ratio F. Note the bifurcations between the different wake modes [88]. Reprinted with the permission of Cambridge University Press.

Hamilton's principle. The equations of motion for the plane frame element are obtained in terms of the displacements and rotations at its nodes. The virtual work of the non-conservative forces acting on the element consists of two components: (1) the mechanical damping, which is represented by a velocity-dependent force; and (2) the aerodynamic damping, which is assumed to have a form similar to that found in Scanlan's model [62]. See Eq. (21).

The response of the structure is obtained by adding up the contributions of each element. A good representation of steady-state vortex-induced vibration behavior is obtained. The extension of the approach to space frame elements (elements of a 3D structure) is readily made and is discussed in the paper.

A finite element analysis of the VIV of a circular cylinder at Reynolds numbers in the range of 100–140 is performed by Nomura [90]. Similarly, Mittal and Kumar [91] use the stabilized space-time finite element method to investigate the VIV of a circular cylinder mounted on lightly damped springs. The cylinder is allowed to vibrate in both the in-line and in the cross-flow directions at $Re = 325$. The behavior of the oscillator for various values of the structural natural

frequency (F_s), including those that are sub- and superharmonics of the natural vortex shedding for the stationary cylinder (F_0), is investigated. In most cases, the trajectory of the cylinder is found to correspond to a Lissajou figure (Fig. 8). For cylinders with effective material density much smaller than that of the surrounding fluid, a region of slight detuning is found to exist in a certain range of F_s values. In this region, the vortex-shedding frequency of the oscillating cylinder does not exactly match the structural frequency. This phenomenon is called "a soft lock-in" by the authors and the detuning is found to vanish if the cylinder density is made much larger than the mass of the surrounding fluid. Similar behavior has been found by the authors in simulations conducted at Reynolds numbers in the range 10^3–10^4 [92].

In a numerical study by Wang et al. [93], a slender elastic cylinder with fixed ends (aspect ratio ≈ 58) in a uniform cross-flow (sub-critical *Re*) is modeled as an Euler–Bernoulli beam. The normal mode method is used to analyze the spanwise structural response in the lift and drag directions. The flow field is resolved using the finite element method. A mesh re-mapping procedure is incorporated to deal with the moving boundary problem which characterizes the free vibration of the cylinder. The results indicate that fluid–structure interactions mainly affect the phase relation between fluid forces and the corresponding vibration of the cylinder. Furthermore, these effects vary along the span of the cylinder.

5. Concluding remarks

A variety of issues concerning the vortex-induced vibration of circular cylinders have been discussed. Selected papers highlighted the influence of vortex-induced unsteady forces on the cylinder, including the phase of the forces relative to the body motion. The phenomenon of lock-in has been discussed and the factors that influence the response of the cylinder (mass and damping) have been listed. The mathematical modeling of vortex-induced oscillations, using nonlinear oscillators and flow-field simulations, has been described. The development in the techniques used to attempt to solve the fully coupled problem, based on the fundamental principles of fluid dynamics and the theory of elasticity, have been illustrated with a few examples from the literature.

In the future, research should be directed towards the better prediction of the dynamic response of structures to VIV. VIV is an inherently nonlinear, self-regulated, multi-dof phenomenon. Vortex shedding gives rise to complex forces. This is only one of a multitude of factors that continues to make VIV prediction in industrial applications substandard. The prediction of VIV requires that one weigh the relative magnitudes of each of these parameters and then try to predict their contribution to the structural response. In the words of Sarpkaya [94], "They [industrial applications] continue to require the input of the in-phase and out-of-phase components of the transverse force, in-line drag, correlation lengths, damping coefficients, relative roughness, shear, waves, and currents, among other governing and influencing parameters, and thus the input of relatively large safety factors". Part of the problem is that different models for the prediction of VIV give different results. As an example, Larsen and Halse [95] find large discrepancies in the predicted response of slender marine structures to vortex shedding when seven different models (e.g., DNV, MARINTEK, SHEAR7) were applied to the same structures under the same environmental conditions. Some of these discrepancies can be attributed to the fact that many of

these models use experimentally obtained values for the flow inputs (e.g., added mass, lift coefficients). Perhaps the advances in the computation of flow–structure interaction (DNS, for example) will one day lead to a better solution. For now, this approach remains hindered by the fact that Reynolds numbers of most industrial applications cannot be simulated.

Better prediction of VIV will hopefully lead to better suppression. However, suppression is in itself a tricky matter. For example, Bearman and Brankovic [96] find that passive suppression devices (strakes and bumps in this case) do not completely eliminate VIV in cylinders with low combined mass and damping, as is often the case in marine applications, this in spite of the fact that helical strakes are used successfully in wind engineering to suppress VIV in chimneys and other slender structures. In addition, it is not possible to completely suppress the vortex-induced vibrations of structures in water by mass redistribution alone [21]. Active control (both open and closed loop) of VIV is an area of significant research activity [97–99] and its outlook looks promising.

Acknowledgements

This work is supported by the Office of Naval Research Grant No. N00014-97-1-0017. We would like to thank our program manager Dr. Thomas Swean for his interest and financial support. We also thank Dr. Timothy Wei for providing some of the figures.

References

[1] S.-S. Chen, *Flow Induced Vibration of Circular Cylindrical Structures*, Hemisphere Publishing Corporation, New York, 1987.
[2] T. Sarpkaya, Vortex induced oscillations: a selective review, *Journal of Applied Mechanics* 46 (2) (1979) 241–258.
[3] S. Krenk, S.R.K. Nielsen, Energy balanced double oscillator model for vortex-induced vibrations, *Journal of Engineering Mechanics* 125 (3) (1999) 263–271.
[4] A. Khalak, C.H.K. Williamson, Motions, forces and mode transitions in vortex-induced vibrations at low mass damping, *Journal of Fluids and Structures* 13 (7–8) (1999) 813–851.
[5] P.W. Bearman, Vortex shedding from oscillating bluff bodies, *Annual Review of Fluid Mechanics* 16 (1984) 195–222.
[6] A. Okajima, A. Nakamura, T. Kosugi, H. Uchida, R. Tamaki, Flow-induced in-line oscillation of a circular cylinder, *European Journal of Mechanics B/Fluids* 23 (2004) 115–125.
[7] M. Matsumoto, T. Yagi, Y. Shigemura, D. Tsushima, Vortex-induced cable vibration of cable-stayed bridges at high reduced wind velocity, *Journal of Wind Engineering and Industrial Aerodynamics* 89 (7–8) (2001) 633–647.
[8] C.C. Chang, M. Gu, Suppression of vortex-excited vibration of tall buildings using tuned liquid dampers, *Journal of Wind Engineering and Industrial Aerodynamics* 83 (1–3) (1999) 225–237.
[9] P. D'Asdia, S. Noe, Vortex induced vibration of reinforced concrete chimneys: in situ experimentation and numerical previsions, *Journal of Wind Engineering and Industrial Aerodynamics* 74–76 (1998) 765–776.
[10] H. Kawai, Bending and torsional vibration of tall buildings in strong wind, *Journal of Wind Engineering and Industrial Aerodynamics* 50 (1993) 281–288.
[11] S.K. Chakrabarti, *The Theory and Practice of Hydrodynamics and Vibration*, World Scientific, Singapore, 2002.
[12] A.P. Dowling, The dynamics of towed flexible cylinders—part 1: neutrally bouyant elements, *Journal of Fluid Mechanics* 187 (1988) 507–532.

[13] M.L. Facchinetti, E. de Langre, F. Biolley, Vortex-induced waves along cables, *Bulletin of the American Physical Society* 46 (2001) 128.
[14] F. Hover, S. Miller, N. Triantafyllou, Vortex-induced vibration of marine cables: experiments using force feedback, *Journal of Fluids and Structures* 11 (3) (1997) 307–326.
[15] J.K. Vandiver, Dimensionless parameters important to the prediction of vortex-induced vibration of long, flexible cylinders in ocean currents, *Journal of Fluids and Structures* 7 (5) (1993) 423–455.
[16] R.H.J. Willden, J.M.R. Graham, Multi-modal vortex-induced vibrations of a vertical riser pipe subject to uniform current profile, in: *Proceedings of the Conference on Bluff Body Wakes and Vortex Induced Vibration*, Port Douglas, Australia, December 2002.
[17] A. Larsen, Generalized model for assessment of vortex-induced vibrations of flexible structures, *Journal of Wind Engineering and Industrial Aerodynamics* 57 (2–3) (1995) 281–294.
[18] C. Christensen, J. Roberts, Parametric identification of vortex-induced vibration of a circular cylinder from measured data, *Journal of Sound and Vibration* 211 (4) (1998) 617–636.
[19] G.J. Lyons, J.K. Vandiver, C.M. Larsen, G.T. Ashcombe, Vortex-induced vibrations measured in service in the Foinaven dynamic umbilical, and lessons from prediction, *Journal of Fluids and Structures* 17 (8) (2003) 1079–1094.
[20] S. Hiejima, T. Nomura, K. Kimura, Y. Fujino, Numerical study on the suppression of the vortex-induced vibration of a circular cylinder by acoustic excitation, *Journal of Wind Engineering and Industrial Aerodynamics* 67–68 (1997) 325–335.
[21] A. Baz, M. Kim, Active modal control of vortex-induced vibrations of a flexible cylinder, *Journal of Sound and Vibration* 165 (1) (1993) 69–84.
[22] A. Marris, A review of vortex streets, periodic wakes, and induced vibration phenomena, *Journal of Basic Engineering* 86 (1964) 185–196.
[23] E. Berger, R. Wille, Periodic flow phenomena, *Annual Review of Fluid Mechanics* 4 (1972) 313–340.
[24] R. King, A review of vortex shedding research and its application, *Ocean Engineering* 4 (1977) 141–172.
[25] K. Billah, A Study of Vortex-Induced Vibration, Ph.D. Thesis, Princeton University, 1989.
[26] M.M. Zdravkovich, Modification of vortex shedding in the synchronization range, *Journal of Fluids Engineering* 104 (1982) 513–517.
[27] T. Sarpkaya, Fluid forces on oscillating cylinders, *Journal of Waterway, Port, Coastal and Ocean Engineering* 104 (1978) 275–291.
[28] R. Gopalkrishnan, Vortex-Induced Forces on Oscillating Bluff Cylinders, Ph.D. Thesis, Massachusetts Institute of Technology and Woods Hole Oceonographic Institution, 1993.
[29] M.L. Facchinetti, E. de Langre, F. Biolley, Coupling of structure and wake oscillators in vortex-induced vibrations, *Journal of Fluids and Structures* 19 (2) (2004) 123–140.
[30] C.H.K. Williamson, The existence of two stages in the transition to three-dimensionality of a cylinder wake, *Physics of Fluids* 31 (11) (1988) 3165–3168.
[31] C.H.K. Williamson, Vortex dynamics in the cylinder wake, *Annual Review of Fluid Mechanics* 28 (1996) 477–539.
[32] C.H.K. Williamson, Advances in our understanding of vortex dynamics in bluff body wakes, *Journal of Wind Engineering and Industrial Aerodynamics* 69–71 (1997) 3–32.
[33] A. Voorhees, T. Wei, Three-dimensionality in the wake of a surface piercing cylinder mounted as an inverted pendulum, in: *Proceedings of the Conference on Bluff Body Wakes and Vortex Induced Vibration*, Port Douglas, Australia, December 2002.
[34] J.C. Lin, D. Rockwell, Horizontal oscillations of a cylinder beneath a free surface: Vortex formation and loading, *Journal of Fluid Mechanics* 389 (1999) 1–26.
[35] J. Sheridan, J.C. Lin, D. Rockwell, Flow over a cylinder close to a free surface, *Journal of Fluid Mechanics* 330 (1997) 1–30.
[36] J. Sheridan, J. Carberry, D. Rockwell, Cylinder wake states—the influence of free surfaces, in: *Proceedings of the Conference on Bluff Body Wakes and Vortex Induced Vibration*, Port Douglas, Australia, December 2002.
[37] D. Rockwell, M. Ozgoren, N. Saelim, Self-excited oscillations of vertical and horizontal cylinders in the presence of a free-surface, in: *Proceedings of the IUTAM Symposium on Integrated Modeling of Fully Coupled Fluid–Structure Interactions Using Analysis, Computations and Experiments*, New Brunswick, NJ, USA, June 2003.

[38] C.H.K. Williamson, A. Roshko, Vortex formation in the wake of an oscillating cylinder, *Journal of Fluids and Structures* 2 (1988) 355–381.
[39] M.M. Zdravkovich, Different modes of vortex shedding: an overview, *Journal of Fluids and Structures* 10 (5) (1996) 427–437.
[40] K. Vikestad, J.K. Vandiver, C.M. Larsen, Added mass and oscillatory frequency for a circular cylinder subjected to vortex-induced vibrations and external disturbance, *Journal of Fluids and Structures* 14 (7) (2000) 1071–1088.
[41] A. Khalak, C.H.K. Williamson, Dynamics of a hydroelastic cylinder with very low mass and damping, *Journal of Fluids and Structures* 10 (5) (1996) 455–472.
[42] C.C. Feng, The Measurement of Vortex-induced Effects in Flow Past Stationary and Oscillating Circular and D-section Cylinders, Master's Thesis, University of British Columbia, 1968.
[43] A. Khalak, C.H.K. Williamson, Fluid forces and dynamics of a hydroelastic structure with very low mass and damping, *Journal of Fluids and Structures* 11 (8) (1997) 973–982.
[44] A. Khalak, C.H.K. Williamson, Investigation of relative effects of mass and damping in vortex-induced vibration of a circular cylinder, *Journal of Wind Engineering and Industrial Aerodynamics* 69–71 (1997) 341–350.
[45] R. Govardhan, C.H.K. Williamson, Modes of vortex formation and frequency response of a freely vibrating cylinder, *Journal of Fluid Mechanics* 420 (2000) 85–130.
[46] R. Govardhan, C.H.K. Williamson, Resonance forever: existence of a critical mass and infinite regime of resonance in vortex-induced vibration, *Journal of Fluid Mechanics* 473 (2002) 147–166.
[47] R. Govardhan, C.H.K. Williamson, Frequency response and the existence of a critical mass for an elastically mounted cylinder, in: *Proceedings of the IUTAM Symposium on Integrated Modeling of Fully Coupled Fluid-Structure Interactions Using Analysis, Computations, and Experiments*, New Brunswick, NJ, USA, June 2003.
[48] P. Dong, H. Benaroya, T. Wei, Integrating experiments into an energy-based reduced-order model for vortex-induced-vibrations of a cylinder mounted as an inverted pendulum, *Journal of Sound and Vibration* 276 (1–2) (2004) 45–63.
[49] E.H. Dowell, Non-linear oscillator models in bluff body aero-elasticity, *Journal of Sound and Vibration* 75 (2) (1981) 251–264.
[50] G. Parkison, Phenomena and modelling of flow-induced vibrations of bluff bodies, *Progress in Aerospace Sciences* 26 (2) (1989) 169–224.
[51] R.E.D. Bishop, A.Y. Hassan, The lift and drag forces on a circular cylinder in a flowing fluid, *Proceedings of the Royal Society Series A* 277 (1963) 32–50.
[52] R.T. Hartlen, I.G. Currie, Lift-oscillator model of vortex induced vibration, *Journal of the Engineering Mechanics* 96 (5) (1970) 577–591.
[53] L. Ng, R.H. Rand, T. Wei, W.L. Keith, An examination of wake oscillator models for vortex-induced vibrations, Technical Report, Naval Undersea Warfare Division, Newport, RI, 2001.
[54] R.A. Skop, O.M. Griffin, A model for the vortex-excited resonant response of bluff cylinders, *Journal of Sound and Vibration* 27 (2) (1973) 225–233.
[55] O.M. Griffin, R.A. Skop, G.H. Koopman, The vortex-excited resonant vibrations of circular cylinders, *Journal of Sound and Vibration* 31 (2) (1973) 235–249.
[56] W.D. Iwan, R.D. Blevins, A model for vortex-induced oscillation of structures, *Journal of Applied Mechanics* 41 (3) (1974) 581–586.
[57] R. Landl, A mathematical model for vortex-excited vibrations of bluff bodies, *Journal of Sound and Vibration* 42 (2) (1975) 219–234.
[58] W.D. Iwan, The vortex induced oscillation of elastic structures, *Journal of Engineering for Industry* 97 (1975) 1378–1382.
[59] R.A. Skop, O.M. Griffin, On a theory for the vortex-excited oscillations of flexible cylindrical structures, *Journal of Sound and Vibration* 41 (3) (1975) 263–274.
[60] W.D. Iwan, The vortex-induced oscillation of non-uniform structural systems, *Journal of Sound and Vibration* 79 (2) (1981) 291–301.
[61] R.A. Skop, S. Balasubramanian, A new twist on an old model for vortex-excited vibrations, *Journal of Fluids and Structures* 11 (4) (1997) 395–412.
[62] E. Simiu, R.H. Scanlan, *Wind Effects on Structures*, Wiley, New York, 1986.

[63] R.I. Basu, B.J. Vickery, Across-wind vibrations of structures of circular cross-section—part 2: development of a mathematical model for full-scale application, *Journal of Wind Engineering and Industrial Aerodynamics* 12 (1) (1983) 75–97.
[64] I. Goswami, R.H. Scanlan, N.P. Jones, Vortex-induced vibration of circular cylinders—part 2: new model, *Journal of Engineering Mechanics* 119 (11) (1993) 2288–2302.
[65] I. Goswami, R.H. Scanlan, N.P. Jones, Vortex-induced vibration of circular cylinders—part 1: experimental data, *Journal of Engineering Mechanics* 119 (11) (1993) 2270–2287.
[66] S.S. Chen, S. Zhu, Y. Cai, An unsteady flow theory for vortex-induced vibration, *Journal of Sound and Vibration* 184 (1) (1995) 73–92.
[67] Y. Cai, S.S. Chen, Dynamic response of a stack–cable system subjected to vortex-induced vibration, *Journal of Sound and Vibration* 196 (3) (1996) 337–349.
[68] H. Gupta, P.P. Sarkar, K.C. Mehta, Identification of vortex-induced response parameters in time domain, *Journal of Engineering Mechanics* 122 (11) (1996) 1031–1037.
[69] O.M. Griffin, G.H. Koopman, The vortex-excited lift and reaction forces on resonantly vibrating cylinders, *Journal of Sound and Vibration* 54 (3) (1977) 435–448.
[70] O.M. Griffin, Vortex-excited cross-flow vibrations of a single cylindrical tube, *Journal of Pressure Vessel Technology* 102 (1980) 158–166.
[71] X.Q. Wang, R.M.C. So, K.T. Chan, A non-linear fluid force model for vortex-induced vibration of an elastic cylinder, *Journal of Sound and Vibration* 260 (2) (2003) 287–305.
[72] C.Y. Zhou, R.M. So, K. Lam, Vortex-induced vibrations of an elastic circular cylinder, *Journal of Fluids and Structures* 13 (2) (1999) 165–189.
[73] H. Benaroya, T. Wei, Hamilton's principle for external viscous fluid–structure interaction, *Journal of Sound and Vibration* 238 (1) (2000) 113–145.
[74] D.B. McIver, Hamilton's principle for systems of changing mass, *Journal of Engineering Mechanics* 7 (3) (1973) 249–261.
[75] H. Benaroya, T. Wei, S. Kuchnicki, P. Dong, Extended Hamilton's principle for fluid–structure interaction, *Proceedings of the Institution of Mechanical Engineers*, *Part K*: *Journal of Multi-body Dynamics* 217 (2003) 153–170.
[76] R.M.C. So, X.Q. Wang, Vortex-induced vibrations of two side-by-side Euler–Bernoulli beams, *Journal of Sound and Vibration* 259 (3) (2003) 677–700.
[77] H. Al-Jamal, C. Dalton, Vortex induced vibrations using large eddy simulation at moderate reynolds number, *Journal of Fluids and Structures* 19 (1) (2004) 73–92.
[78] I. Jadic, R.M.C. So, P. Mignolet, Analysis of fluid–structure interactions using a time-marching technique, *Journal of Fluids and Structures* 12 (6) (1998) 631–654.
[79] C. Evangelinos, Parallel Simulations of Vortex-Induced Vibrations in Turbulent Flow: Linear and Non-Linear Models, Ph.D. Thesis, Brown University, 1999.
[80] M. Tutar, A.E. Holdo, Large eddy simulation of a smooth circular cylinder oscillating normal to a uniform flow, *Journal of Fluids Engineering* 122 (4) (2000) 694–702.
[81] J.R. Meneghini, P.W. Bearman, Numerical simulation of high amplitude oscillatory flow about a circular cylinder, *Journal of Fluids and Structures* 9 (4) (1995) 435–455.
[82] T. Sarpkaya, Computational methods with vortices, *Journal of Fluids Engineering* 111 (1) (1989) 5–52.
[83] T. Sarpkaya, Vortex element methods for flow simulation, *Advances in Applied Mechanics* 31 (1994) 113–247.
[84] C. Evangelinos, D. Lucor, G.E. Karniadakis, DNS-derived force distribution on flexible cylinders subject to vortex-induced vibration, *Journal of Fluids and Structures* 14 (3) (2000) 429–440.
[85] E. Guilmineau, P. Quetey, A numerical simulation of vortex shedding from an oscillating circular cylinder, *Journal of Fluids and Structures* 16 (6) (2002) 773–794.
[86] R.H.J. Willden, J.M.R. Graham, Numerical prediction of VIV on long flexible circular cylinders, *Journal of Fluids and Structures* 15 (3–4) (2001) 659–669.
[87] H.M. Blackburn, R.N. Govardhan, C.H.K. Williamson, A complementary numerical and physical investigation of vortex-induced, *Journal of Fluids and Structures* 15 (3–4) (2000) 481–488.
[88] H.M. Blackburn, R.D. Henderson, A study of the two-dimensional flow past an oscillating cylinder, *Journal of Fluid Mechanics* 385 (1999) 255–286.

[89] H. Barhoush, A.H. Namini, R.A. Skop, Vortex shedding analysis by finite elements, *Journal of Sound and Vibration* 184 (1) (1995) 111–127.
[90] T. Nomura, Finite element analysis of vortex-induced vibrations of bluff cylinders, *Journal of Wind Engineering and Industrial Aerodynamics* 46–47 (1993) 587–594.
[91] S. Mittal, V. Kumar, Finite element study of vortex-induced cross-flow and in-line oscillations of a circular cylinder, *International Journal for Numerical Methods in Fluids* 31 (1999) 1087–1120.
[92] S. Mittal, V. Kumar, Flow-induced vibrations of a light circular cylinder at reynolds numbers 1000 to 10,000, *Journal of Sound and Vibration* 245 (5) (2001) 923–946.
[93] X.Q. Wang, R.M.C. So, Y. Liu, Flow-induced vibration of an Euler–Bernoulli beam, *Journal of Sound and Vibration* 243 (2) (2001) 241–268.
[94] T. Sarpkaya, A critical review of the intrinsic nature of VIV, *Journal of Fluids and Structures* 19 (4) (2004) 389–447.
[95] C.M. Larse, K.H. Halse, Comparison of models for vortex induced vibrations of marine structures, *Marine Structures* 10 (6) (1997) 413–441.
[96] P. Bearman, M. Brankovic, Experimental studies of passive control of vortex-induced vibration, *European Journal of Mechanics B/Fluids* 23 (2004) 9–15.
[97] L. Cheng, Y. Zhou, M.M. Zhang, Perturbed interaction between vortex shedding and induced vibration, *Journal of Fluids and Structures* 17 (7) (2003) 887–901.
[98] M.M. Zhang, L. Cheng, Y. Zhou, Closed-loop control of fluid–structure interaction on a flexibly supported cylinder, *European Journal of Mechanics B/Fluids* 23 (2004) 189–197.
[99] N. Fujisawa, T. Nakabayashi, Neural network control of vortex shedding from a circular cylinder using rotational feedback oscillations, *Journal of Fluids and Structures* 16 (1) (2002) 113–119.